AN INVESTIGATION OF THE HYDRAULICS IN A PROTOTYPE POOL-AND-CHUTE, VORTEX WEIR FISHWAY FOR ANADROMOUS FISH PASSAGE.

By

Brendan Michael Foster

A Thesis Presented to

The Faculty of Humboldt State University

In Partial Fulfillment of the Requirements for the Degree

Master of Science in Environmental Systems: Environmental Resources Engineering

Committee Membership

Dr. Margaret Lang, Committee Chair

Dr. Eileen Cashman, Committee Member

Dr. Mark Henderson, Committee Member

Dr. Rick Zechman, Program Graduate Coordinator

July 2017

ABSTRACT

AN INVESTIGATION OF THE HYDRAULICS IN A PROTOTYPE POOL-AND-CHUTE, VORTEX WEIR FISHWAY FOR ANADROMOUS FISH PASSAGE.

Brendan Michael Foster

This thesis presents the hydraulic characteristics and simulated passage efficiency of a hybrid pool-and-chute, vortex weir fishway designed by Michael Love & Associates. A physical 1:15 scale model was constructed and evaluated at an 8% slope over three prototype flow rates representing high and medium fish passage flows. The highest velocities and turbulent kinetic energy (TKE) values were concentrated along the fishway centerline at the high and medium flow rate and the pool sides showed lower velocities and TKE. Large eddies spin laterally and longitudinally throughout each pool. The velocity vector directions at the lowest flow rate measured differed from the two higher flow rates with larger, more pronounced eddies on the pool sides.

The fishway's velocities and their spatial distribution were used to estimate passage success and fatigue level. A preliminary numerical model was created that simulates a steelhead or coho salmon ascending the fishway. This model uses observed size distributions for adult steelhead and coho from data presented in the literature and calculates each individually sampled fish's passage time and percent fatigue. Two swim pathways were analyzed at both the high and medium flow rates. A thousand fish of each species were simulated ascending the fishway, and zero fish reached 100% fatigue under

any scenario. Results indicate that ascension of the prototype fishway should not be energetically limiting for steelhead or coho salmon.

This model was also used to calculate the maximum fishway length (holding the original 30-feet width constant) over which zero fish reached 100% fatigue, assuming fish did not rest and recover from fatigue within the pools between weirs. Results indicate the fishway length could increase by an additional three pools and weirs or 37.5 feet without causing any fish in the sample distribution to reach 100% fatigue. Conservative fishway design would not recommend increasing the fishway length beyond the length where fish reach 100 F% to ensure an energetic factor of safety and account for potential behavioral or motivation delays. Further investigation into the nature of fish use of the new prototype fishway design could help calibrate the models presented in this thesis and increase the accuracy of the passage efficiency estimations.

ACKNOWLEDGEMENTS

Foremost, I would like to thank my advisor and committee chair, Dr. Margaret Lang, for her support, guidance, and dedication. Completion of this thesis would simply not have been possible without her. Next, I would like to thank my committee member Dr. Eileen Cashman for her invaluable feedback and advice. I would also like to thank my committee member Dr. Mark Henderson for his thoughtful commentary which has increased the value of this work.

Many other individuals and groups outside of my thesis committee have made important contributions. I would like to thank Michael Love & Associates located in Arcata, California, especially Michael Love and Travis James. I would like to extend special thanks to Michael Love for the numerous consultations throughout the entire process that significantly enhanced the value of this work. I would like to thank everyone at Humboldt State University, including Marty Reed, Colin Wingfield, Mathew Nyberg, Brian Draeger, Brian Weekly, and Neftali Eunice Romero. Next, I would like to thank my friends Alan Sanchez, Andrew Sanchez, Anthony Sanchez, Jake Rada, and Emily McDougal. Finally, I would like to thank my family for their constant love, support, and encouragement, most of all my parents Michael and Holly Foster, and my sisters Jillian and Whitney Foster.

I must also acknowledge the financial support from Michael Love & Associates that made this research possible.

TABLE OF CONTENTS

LIST OF TABLES

LIST OF FIGURES

INTRODUCTION

Research Context

Anadromous fishes reproduce in freshwater streams then their progeny migrate to the ocean where they grow and mature before returning to freshwater streams to complete their life cycle by spawning the next generation. These fish encounter numerous barriers during their freshwater migration. Migration barriers such as dams, water storage projects, irrigation diversions, and impassable culverts are significant factors affecting most anadromous fish populations. According to the National Marine Fisheries Service (NMFS, 2008) the primary effects of barriers on anadromous fishes are the reduction of their population abundance and productivity through excessive mortality, and reduction in habitat quantity and quality. Fishways are ubiquitous structures used to mitigate the adverse effects of migration barriers.

Towler et al. (2015) defines a fishway as hydraulic structures that create continuous pathways for fish to move over or around otherwise impassable barriers. Many existing fishways were designed for adult fish. Designing fishways for multiple species and life stages is of growing interest in the United States, Canada, and other countries. However, rivers managed for multiple target species require fish passage solutions that accommodate wide ranges of fish sizes, swimming abilities, and migration strategies (Bunt et al., 2012).

Additionally, current fishway designs have been shown to possess attributes that hinder their ability to attract fish to enter a fishway, pass fish, or both. Two meta-analyses of existing peer-reviewed scientific papers conducted by Bunt et al. (2012) and Noonan et al. (2012) compared attraction and passage efficiency of four common fishway designs including: pool and weir, vertical slot, Denil, and nature-like. These analyses showed that designs with high entrance rates had low passage rates, and vice versa. For instance, pool-and-weir type fishways showed high entrance rates, but low passage rates, while nature-like fishways showed low entrance rates, but high passage rates. These correlations are hypothesized to be a result of the hydraulics not optimally accommodating the behavioral and hydraulic preferences of the target species. A solution proposed to rectify this issue was the design of hybrid fishways that incorporate elements from multiple designs to both attract and pass fish efficiently.

The research goal of this thesis is to measure the hydraulic performance of a scale model of a new pool-and-chute fishway designed by Michael Love and Associates (MLA). This new hybrid design is intended to promote passage not only for adult anadromous salmonids but also juvenile salmonids and non-salmonid species, especially lamprey. The end product of this analysis is quantifying the hydraulic performance characteristics in terms of velocity vectors, turbulence characteristics and statistics, and flow type (plunging, transitional, or streaming), over a range of passage flows, and determining where passage is potentially possible for adult salmonids. The fishway was designed for steelhead (*Oncorhynchus mykiss*) passage in Alameda Creek, a tributary to southern San Francisco Bay, but this thesis also evaluates passage for adult coho salmon

(*Oncorhynchus kisutch*). With additional data, the model developed for this analysis could be calibrated and used to evaluate fishway performance and design, and for additional species.

Pool-and-chute fishways have had limited hydraulic verification to date because they have a short history and have not been extensively used or evaluated (CDFW, 2009). Thus, research aimed at quantifying and characterizing the hydraulics of this new pool-and-chute fishway design is merited.

Design

The proposed full-scale fishway is designed to operate over a range of flows between 20 and 181 cubic feet per second (cfs), a slope of 8%, and is 144-ft long x 30-ft wide. The design includes a vortex weir configuration which has been observed to yield better flow conditions for fish passage compared to other designs by minimizing water surface elevations between pools and concentrating turbulence (Allen et al., 2004). The new vortex pool-and-chute hybrid design has V-shaped in the longitudinal direction with the apexes located in the upstream direction. The apex of the weirs converges to a chute located in the center of the weirs that is placed perpendicular to flow. Each weir slopes up in the lateral direction towards the side walls. The design also includes orifices intended to improve sediment transport capacity and lamprey passage (Love, 2015).

Research Questions

This thesis investigates five questions pivotal to the success of the proposed fishway. Answers to these questions require understanding of the fishway hydraulics and determining where passage is possible over the desired range of flows.

1. What are the velocity magnitudes and directions throughout each of the fishway pools for three flows within the fish passage flow range and especially at the high fish passage flow?
2. What are the turbulent kinetic energy values throughout each pool of the fishway and do these show that energy dissipation is spatially limited to allow calmer areas within each pool?
3. What are the potential migration pathways for steelhead and coho salmon passage?
4. What are the estimated percent fatigue and ascension times for adult salmonids to ascend the prototype fishway?
5. How long can this prototype fishway be before adversely affecting passage efficiency?

Impacts

Although the physical model studied was for a fishway designed specifically for steelhead passage in Alameda Creek, California, answers to these research questions are also relevant for engineers, fish biologists, ecologists, and managers interested in installing similar fishway designs in other locations. The design should have good transferability and could be a preferred alternative to other designs, especially for coastal freshwater streams on the Pacific Coast.

BACKGROUND

Introduction

The background section summarizes the current literature as it relates to the design of pool-and-chute fishways. The background is divided into six sections. The first section examines fish passage design flows and standard methods for their calculation. The second section briefly describes the three fish swim modes. The third section summarizes generally accepted fishway flow regimes and their attributes. The fourth section presents design characteristics for pool-and-weir and roughened-chute fishways, the two fishway types that a pool-and-chute fishway is based on. The fifth section explains the importance of velocity and its relationship to fish swimming speeds and fatigue times. The sixth section presents the physiological and behavioral effects of turbulence on fish, and our understanding of how to characterize this effect.

Fish Passage Design Flows

Providing passage at all flow rates for a given system is usually not practical or necessary. Using a hydraulic approach, a fishway should satisfy fish passage criteria within a range of fish passage design flows. The low and high passage design flow objectives are to maintain sufficient depth, and avoid exceedingly high water velocities and turbulence, respectively (CDFW, 2009).

When determining the range of fish passage flows, the flows that fish typically migrate upstream based on the life history of the target fish are considered. Upstream movement for adult salmonids occurs near the end of their life cycle at the time of their spawning migration. While juvenile salmonids may move upstream occasionally for daily foraging or due to varying flows, overcrowding or poor water quality (CDFW, 2009).

California Department of Fish and Game (CDFG) (2002) criteria and National Oceanic and Atmospheric Administration (NOAA) (2001) guidelines recommend specific criteria for fish passage design flows. These guidelines assert that fish passage design flows consider the hydrologic characteristics of the stream and the sensitivity of those characteristics to cause delays in movement. Swimming capabilities vary between species and within the same species, which makes it difficult to accommodate many different fishes. If fish encounter a structure that is a high-flow barrier, migration may be delayed until flow subsides. Such a delay can directly affect the ability of fish to spawn, locations that they can spawn, and the viability of their offspring. Lang et al. (2004) discusses the considerations necessary for developing appropriate fish passage design flows and investigates the consequences of migration delay with specific design flows. This research increased our understanding of fish use of passage facilities during specific flows and improved the flow criteria for fish passage engineering design in California.

The standard method for determining the fish passage design flow range is to create a flow duration curve for the specific location. For large drainages, a common upper fish passage design flow for salmonids is the 10% exceedance flow during their migration period. A 10% exceedance flow is the flow rate that is equaled or exceeded

10% of the time during the period of migration for the target species (Love & Llanos, 2006). In northern and central California adult steelhead commonly begin their upstream migration during high flow events between December and March. Since a significant number of fish were found to be attempting to migrate at flows above the 10% exceedance flow, California and other states have changed the upper fish passage design flow to the annual 1% exceedance flow (Lang, et al., 2004).

Fish Swim Modes

It is generally accepted that fish possess three different swimming speeds; burst, prolonged, and sustained (CDFW, 2009; NMFS, 2008). The fastest speed, commonly called a fish's burst speed, is normally used to swim through faster than average water velocities and to evade predators. Fish can only maintain burst speed for a very brief time which is usually followed by a period of rest. Prolonged speeds are significantly slower than burst speeds, but are the next fastest. Prolonged swim speeds are used by fish in quick moving reaches and to overcome small rapids. Sustained speeds, are the slowest speed and can be maintained for long periods of time. Sustained speed is used while feeding or moving through slow reaches (Clay, 1995). Different fishway designs require fish to swim in different modes. For example, some short spanned Denil fishways are designed for fish to use burst swim mode for the entire ascension during fish passage design flows. Whereas pool-and-weir fishways are designed for fish to be able to use multiple swim modes in their ascension during fish passage design flows.

Flow Regime

Over the range of fish passage flows, hydraulic conditions within a pool-and-chute fishway will vary. At low flows, the water plunges over the weir, and as flow increases, the hydraulic condition transitions to intermediate states of flow. Clay (1961) provided one of the earliest detailed descriptions of the plunging, transitional, and streaming flow regimes for a pool-and-weir fishway. Ead et al. (2004) confirmed these results by directly measuring 435 water surface profiles in a scale pool-and-weir fishway model in a laboratory flume. These water surface profiles were measured over numerous flow rates to best identify the small differences between flow regimes and the different types of flows within each regime. The flow regimes were further defined by Ead et al. (2004) using dimensionless discharge quantities and weir geometry. Figure 1 shows a graphic interpretation of plunging, transitional, and streaming flow regimes recreated from drawings by Ead et al. (2004) for a pool-and-weir fishway.

On one end of the spectrum there is plunging flow which is characterized by a circular pattern of flow upstream of the weir which creates a layer of water that flows over the weir, a nappe, that plunges down to the bottom of the fishway. Then, it moves downstream adjacent to the bottom and elevates upwards when it nears the next weir before going over the weir or back upstream on the surface of the pool. When flow is plunging, the water elevation in the downstream pools is generally below the upstream weir crest (Ead et al., 2004).

When flows were increased, the hydraulics in the pool-and-weir fishway transitioned through a range of conditions ending with a streaming flow regime. In streaming flow conditions, there is a continuous surface jet that passes over the weirs and skims over the surface of the pools. The shear forces in the pools create a circulation pattern in the opposite direction of the plunging flow regime (Ead, et al., 2004).

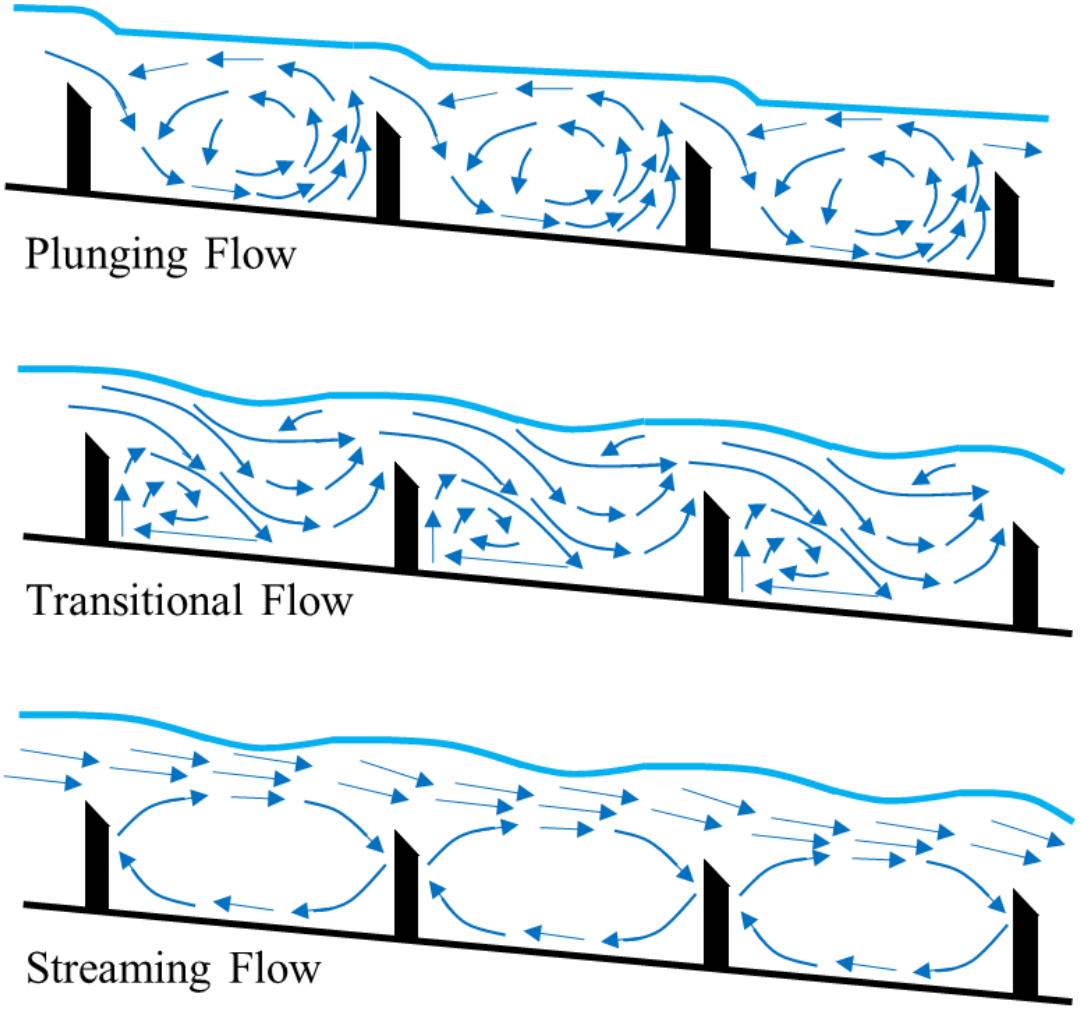

Figure 1. Drawings of plunging, transitional, and streaming flow regimes for a pool-and-weir fishway, recreated from Ead et al. (2004).

When bed slope, weir spacing, and height are varied, additional transitional regimes exist. In pool-and-weir fishways, the weirs are relatively close to each other thus they act together hydraulically. Ead et al. (2004) created sketches of the various plunging, transition, and streaming flows. The transitional flow regime depicted in Figure 1 is representative of the five different transitional flow regimes which are individually detailed in Ead et al. (2004).

Nyberg et al. (2016) conducted preliminary analyses on this new pool-and-chute fishway model designed my Michael Love & Associates to confirm the presence of streaming and plunging flow regimes as expected and define the flows for transition or percent of each. At higher flows, there is a streaming flow moving quickly down the center of the weirs, and slower plunging flow going over the weir on both sides of the stream in the center. At lower flows, there is only plunging flow. The location and quantity of streaming and plunging flow changes with flow rate.

Fishway Designs

Pool-and-weir fishway

Pool-and-weir fishways consist of multiple pools created by a series of weirs (Figure 2). The pools allow fish to rest, before swimming over or through the plunging flow at the weirs where they encounter the most difficult passage conditions of minimum water depths, and maximum water velocities within the fishway (Bates, 1991). After resting in the pools using sustained and prolonged swim mode, fish ascend pool-and-weir

fishways by using their burst speed and swimming or jumping over the weirs (Ead et al., 2004). They are usually designed to allow fish migration over a specific range of flows and must have an entry with suitable fish attraction, minimize water surface differences between adjacent fishway pools, and maintain sufficient pool volumes to dissipate energy between pools.

Figure 2. Image of Pool-and-weir fishway on the Grand River in Grand Rapids, Michigan (Michigan Department of Natural Resources, 2017).

Generally, pool-and-weir fishways function efficiently only over a narrow range of flows because they are effective at passing fish when plunging flow hydraulics are present. As flow increases, the turbulence levels in the pools also increase and can reach a level that is too high for fish passage. As the weirs become submerged, the hydraulic regime transitions from plunging to streaming flow. Once streaming flow begins in a

pool-and-weir fishway it can easily turn into a barrier due to exceedingly high velocities. To mitigate the adverse effects of high flows, pool-and-weir fishways are often designed with a bypass weir to divert some of the flow around the fishway and thus maintaining a plunging flow regime for a longer period of time and over a larger range of flows (Love & Llanos, 2006).

Roughened chute fishway (Denil and Alaskan Steeppass fishways)

Roughened chutes are tall and narrow fishways usually made out of steel or wood and may be placed at slopes as high as 20%. They have tightly spaced baffles along the floor and vertical baffles that go up to the top of the side walls. High amounts of turbulence are created in roughened chute fishways and this decreases velocities and maintains sufficient depth. The most common types of roughened chute fishways are the Denil and Alaskan Steeppass (ASP) (CDFG, California Department of Fish and Game. 1998). The Denil is an artificially roughened channel that has historically been very popular throughout the world. However, the Denil fishway is not commonly used in the Pacific Northwest due to its narrow fish passage flow range and susceptibility to debris blockages (Bates, 2001). Figure 3 shows an example of a typical Denil fishway.

Figure 3. Image of A typical Denil fishway on the Salmon Falls River, South Berwick, Maine (Kleinschmidt, 2017).

The ASP fishway is a specific type of Denil fishway originally designed for installations in remote locations or sites with poor access. ASP fishways are used in the Pacific Northwest primarily as a structure for trapping and evaluating fish, but are also used as temporary passage facilities, and at small falls and low-head dams. The ASP controls velocities more effectively than the Denil because the baffles are angled upstream into the flow. However, there is a greater concern with debris blockages and limited fish passage flow range because it has smaller open dimensions. Figure 4 shows a typical ASP fishway with its unique baffle configuration on the left, and an example of its limited range of fish passage flows on the right (Love & Llanos, 2006).

Figure 4. Image of A typical ASP fishway shown without water from the upstream end (left) to see baffle configuration, and with water from the downstream end (right) to see the baffles effects (Alaska SteepPass Fishways by Sheepscot Machine Works, 2017).

Pool-and-chute fishway

The standard pool-and-chute fishway design includes straight, non-angled weirs that slope upward towards the sidewalls. A notch is removed in the center of each weir to exploit the chute portion of the fishway. Pool-and-chute fishways exploit the advantages of several currently used designs including pool-and-weir, Denil, and ASP fishways. At low fish passage flows, they operate as a pool-and-weir fishway, and at moderate to high fish passage flows streaming flow is concentrated down the centerline of the fishway and plunging flow occurs adjacent to the streaming flow at the sides. This allows fish to ascend the fishway along the sides where there are lower velocities and less turbulence, while a large amount of the flow streams down the centerline. Concentrating streaming flow in the centerline, gives pool-and-chute fishways a wider range of fish passage flows. Streaming flow down the center of the fishway also offers excellent attraction for fish and

passage for debris. Pool-and-chute fishways are often designed to laterally span the entire channel, which eliminates concerns about sufficient attraction flow and the need for a bypass weir (Love & Llanos, 2006).

Bates (1991) conducted one of the first hydraulic investigations of a pool-and-chute fishway. The lateral slope of the baffles controls the width of the passage corridor over the weir by controlling the width of streaming flow and establishes the high fish passage design flow. The steeper the lateral baffle slope, the narrower the passage corridor but the higher the high fish passage design flow rate. Steeper lateral baffle slopes make the weir height very high near the side walls making it difficult to ascend, but also concentrates high flows more making the velocities at the sides of the pools lower even at higher flows. Plunging flow allows fish passage near the walls and adjacent to the high velocity attraction jet. Plunging flow is reinforced by the shape of the weir crests and orifices. Figure 5 shows a standard pool-and-chute fishway design, without orifices on the bottom of the weirs. It also shows its ability to manage flows, to keep faster velocities along the center chute and slower velocities in the sides of the pools.

Figure 5. Image of A standard design, partially spanning pool-and-chute fishway in San Anselmo Creek, Marin County, California (Michael Love and Associates, 2012).

Velocity

Velocity plays an important role in the design and success of fishways because zones of high-velocity flow may create velocity barriers that exceed the physical and behavioral capabilities of fishes and thus, prevent passage. However, higher velocities are needed for attraction. A higher velocity jet at the fishway entrance is often used to help fish locate the fishway entrance and make it compelling enough for them to decide to enter. Fishways are sometimes intentionally designed to contain areas with high

velocities which simultaneously allows other areas to sustain lower velocities. This creates continuous pathways through the fishway with low velocities over a wider range of flows (Haro et al., 2004). Velocity is one of the most investigated hydraulic parameters affecting fish passage because it has an important role in determining a particular fish species ability to migrate through the fishway.

For design considerations, mean water velocities must remain below the target species burst speed through the fastest moving sections of the fishway, and below the target species sustained swimming speed through the rest of the fishway. Fish can only maintain the sustained swim speed for minutes (Clay, 1995). After exceeding that time fish must rest before ascending to the next pool. Fishway designs seek to reduce velocities below the maximum swim speeds of target species. To reduce velocities, energy is dissipated by increasing turbulence. The challenge in fishway design is to achieve sufficiently low velocities while simultaneously maintaining turbulence at levels low enough to allow passage (Towler et al., 2015).

Turbulence and Energy Dissipation Factor

Turbulence has been defined as a spatially complex distribution of vorticities which advects chaotically in accordance with vorticity and angular momentum. The vorticity field is random in space and time, and exhibits a wide and continuous distribution of length and time scales (Davidson, 2015; Kirkbride, 1993; Warhaft, 2002). Turbulence arises as a result of shear being greater than the viscous effects in velocity

gradients, which are largely created by interactions between the flow and instream structures of the stream bed of protuberances (Tritico, 2009).

Turbulence has been observed to have a large influence on the swimming performance of fish, their resting positions, and selection of habitat (Liao, 2007; Tritico, 2009; Webb & Cotel, 2010; Lacey et al., 2012). The effect of turbulence on fish kinematics and behavior is complex. Different levels of turbulence affect species differently and within a particular species will affect some fish more than others. It is generally accepted that there are benefits and costs to higher levels of turbulence. High levels of turbulence can increase the locomotive cost of fish (Liao, 2007) because the fish must use more energy to stabilize themselves within the turbulence and swim past the area. Extremely high levels of turbulence can disorient, exhaust, or injure a fish, creating a barrier. Smaller fish, have less mass and are weaker swimmers, making them more susceptible to the effects of turbulence (CDFW, 2009). However, many studies have shown that fish can decrease the locomotive cost by exploiting turbulence in hydraulic structures (Webb, 1998; Hinch & Rand, 2000; Liao et al., 2003; Montgomery et al., 2003; Smith, 2003). Fish can maximize these exploitations when turbulence in hydraulic structures remain steady and predictable (Liao, 2007).

Turbulent kinetic energy (TKE) is one direct measure of the total turbulent energy production due to turbulent fluctuations in the flow (Hockley et al., 2013). It is important for developing turbulence models and is useful for understanding how the mean flow moves kinetic energy through a turbulent flow structure. TKE may be calculated as (Lacey et al., 2012):

$$TKE = \frac{1}{2}({u_{rms}}^2 + {v_{rms}}^2 + w_{rms}^2) \quad [1]$$

Where:

$u_{rms}, v_{rms}, and\ w_{rms}$ are the root-mean-squared (RMS) values of the velocity components in the streamwise, normal, and vertical directions, respectively.

METHODS

The methods section describes the experimental procedure used to test the hydraulics of the scale model. The model experiments were conducted in the 40-ft (12-m) long by 2.5-ft (0.75-m) wide, variable slope sediment transport flume at Humboldt State University (HSU). First, the model construction and application of the similarity rules are presented. Then, calibration of the v-notch weir in the sediment transport flume to obtain accurate flow measurements is explained. Next, the Acoustic Doppler Velocimeter (ADV) data collection and processing are summarized and discussed. This section goes on to describe how turbulent kinetic energy was calculated, and how and why the point velocity vector data were visually confirmed. The final section explains the techniques used to model the migration pathways, and conduct Monte Carlo simulations of fish attempting to pass the simulated fishway through two routes at the high and medium flow rates.

Design

To study the proposed fishway design by Michael Love & Associates, the Humboldt State University (HSU) College of Natural Resources and Sciences (CNRS) technicians and Environmental Resources Engineering (ERE) students built a 1:15 scale model of the prototype fishway. The design includes eleven weirs which create ten pools, and each weir has two orifices located on the bottom of each of the lateral baffles. A

schematic of the scale model is shown in Figure 6. The model was constructed of acrylic to have an approximate scaled-up roughness value matching the prototype material, concrete. The fishway model was placed in the sediment transport flume at HSU where all measurements were performed. The model was developed to be geometrically similar and have an equivalent time scale ratio (kinematic similarity) as the prototype by applying geometric and Froude scaling.

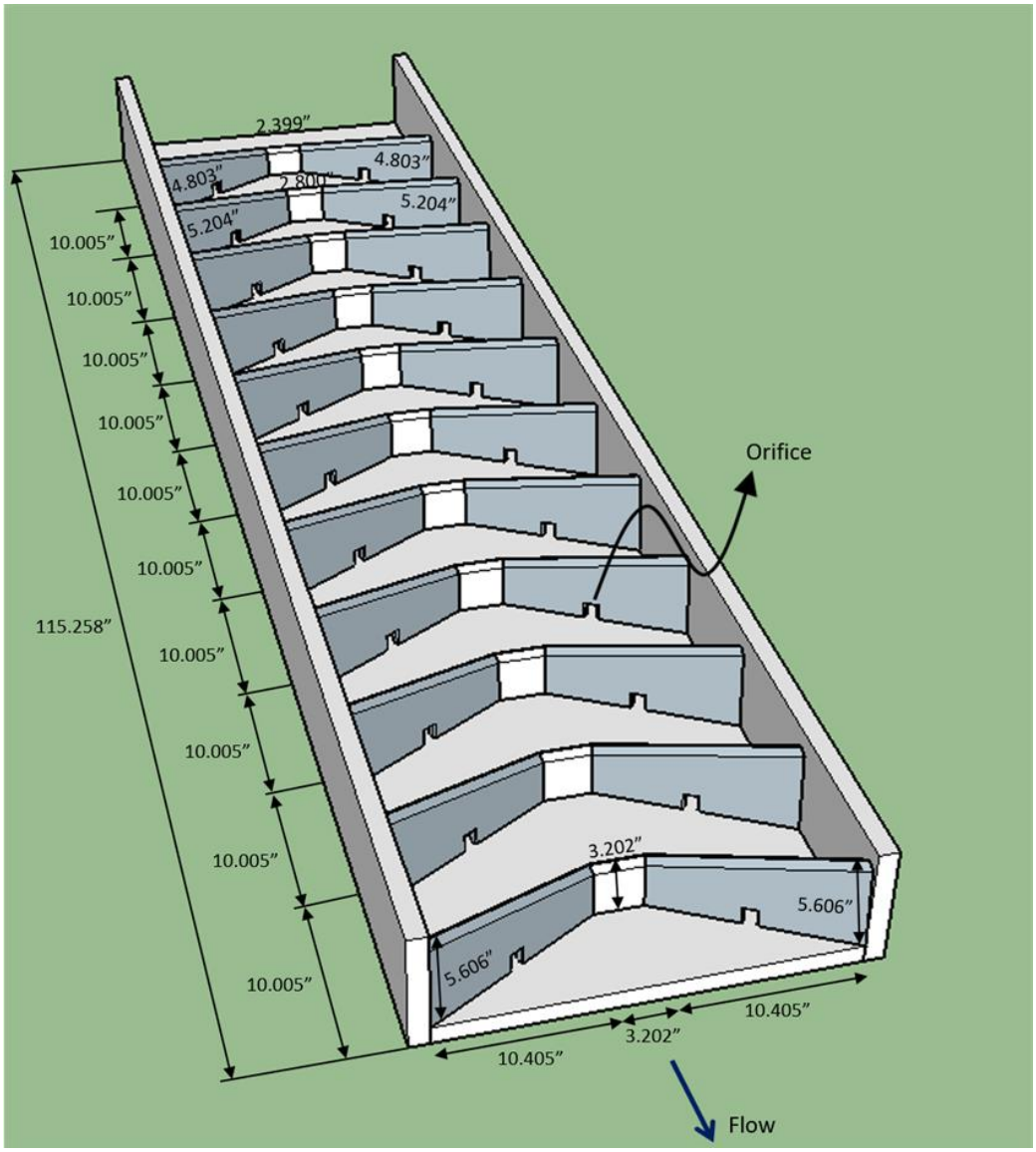

Figure 6. Schematic of Fishway Scale Model.

Geometric scaling ensures all slopes and angles are maintained between model and prototype by maintaining the same linear scale ratio in the x-, y-, and z- directions. The length scale relationship for geometric scaling is given as (White, 2011):

$$L_m = \alpha L_p \qquad \text{where: } \alpha = \frac{1}{15} \qquad [2]$$

Froude scaling was applied to account for the effects of gravitational and inertial forces, which dominate turbulent fluid flow in open channels (Houghtalen et al., 2010). The relationship may be expressed as (White, 2011):

$$\mathrm{Fr}_{\mathrm{m}}^{2} = \mathrm{Fr}_{\mathrm{p}}^{2} \quad [3]$$

$$\frac{\mathrm{V}_{\mathrm{m}}^{2}}{\mathrm{gL}_{\mathrm{m}}} = \frac{\mathrm{V}_{\mathrm{p}}^{2}}{\mathrm{gL}_{\mathrm{p}}} \quad [4]$$

From Equation [4], the velocity scaling between model and prototype is:

$$\frac{\mathrm{V}_{\mathrm{m}}}{\mathrm{V}_{\mathrm{p}}} = \sqrt{\frac{\mathrm{L}_{\mathrm{m}}}{\mathrm{L}_{\mathrm{p}}}} = \sqrt{\alpha} \quad [5]$$

Utilizing Equations [2] and [5], the flow rate scale can be derived:

$$\frac{Q_m}{Q_p} = \frac{\mathrm{V}_{\mathrm{m}}\mathrm{L}^{2}{}_{\mathrm{m}}}{\mathrm{V}_{\mathrm{p}}\mathrm{L}^{2}{}_{\mathrm{p}}} = \sqrt{\alpha}\,(\alpha^{2}) \; = \alpha^{5/2} \quad [6]$$

The model flow rates can thus be related to the field-scale, prototype design flows as:

$$Q_m = \alpha^{5/2} Q_p \quad [7]$$

Flume V-notch Weir Calibration

The V-notch weir used to measure flow through the sediment transport flume was calibrated to confirm that flow readings were accurate. A stopwatch, bucket, and scale were used to calculate the flow through the V-notch over a range of water elevations in the flume head tank. The water leaving the v-notch weir filled the bucket and was timed. The captured water weight was measured, and using the specific weight of water,

converted into a volume. The flow rate was thus calculated as volume divided by the measured elapsed time. A rating curve was created and, using Microsoft Excel, a regression analysis was performed to fit an equation to the curve. The residuals were also analyzed to determine where flow calculations were most sensitive to water elevation changes.

Flow Rates and Slope

Velocity measurements were collected at three flow rates representing prototype flow rates of 181, 144, and 107 cfs and are referred to in this thesis as the high, medium, and, low flow rates, respectively. The high flow rate was chosen because it represents the high fish passage design flow rate for the prototype fishway. The actual low fish passage design flow rate is around 20 cfs, but the medium and low flow rates evaluated for this model study were chosen to provide a range of flow rates where passage is thought to be more challenging. The fishway slope was held constant at 8% to mimic the slope of the site on lower Alameda Creek. The tailwater depth was held constant at 4.5 inches above the fishway bottom for all flows which pooled water about half way up the entrance weir. The tailwater depth was adjusted by applying an adjustable flap gate downstream of the model that creates a pool between the gate and the downstream end of the model.

Acoustic Doppler Velocimetery Data Collection

Due to low water depths through the model a 2-D, side-looking Acoustic Doppler Velocimeter (ADV) was used to collect 2-D velocity data at three pool depths throughout the fishway. ADV's measure velocities of water using the Doppler effect. An ADV transmits a sound wave that is reflected by suspended particles in the fluid. The sound waves are focused on a 1 cm^3 sampling volume located 10 cm from the transmitter. The magnitude of the Doppler shift of the reflected waves is used to estimate the magnitude of the velocity vector components (SonTek, 1997). The amount that the initial sound wave with known frequency has been shifted is represented by (SonTek, 2001):

$$F_{doppler} = -F_{source}\left(\frac{V}{C}\right) \quad [8]$$

Where V is the relative speed between source and receiver (SonTek, 2001).

The ADV used is 60 cm long with the transmitter and receiver at one end, one centimeter from the bottom. The transmitter is directly at the bottom 59 cm down and the receivers are angled at 120-degrees apart. The ADV transmits at a frequency of 10 Hertz and measures the velocity vector components in the x- and y- directions but not the z-direction. A custom rail mount shown in Figure 7 was built by CNRS technicians and used to hold the ADV for measurements. It can be adjusted, manually to place the ADV in any position along the length, width or depth of the flume. The ADV head can also be rotated to measure in any orientation within a horizontal plane.

Figure 7. Image of ADV on mount and rails shown collecting a velocity measurement in model fishway.

A Cartesian coordinate system was established along the fishway with the origin at the most upstream edge of the model on the right side of the fishway when looking downstream. The coordinate system origin and orientation can be seen in Figure 8. All measurements collected in the fishway were defined in these coordinates.

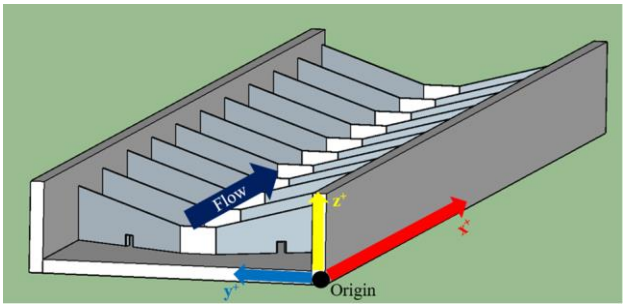

Figure 8. Image of Cartesian coordinate system for position measurements in x-, y-, and z- directions.

Fourteen measurement locations were arranged in a gridded pattern in the pools between each weir and the same grid was used for all three flow rates. For each location,

a measurement was made at the surface, middle, and bottom of the water column for a total of 42 point velocity measurements per pool. Location of the vertical positions for the surface and middle points were adjusted as flow depth varied. All measurements at the bottom depth were located approximately one centimeter above the pool bottoms. The measurements collected at the surface were approximately two centimeters below the water surface to ensure a reliable measurement. The vertical distance between the bottom and surface measurement depths, h, was used to calculate the middle depth by dividing h in half. Figure 9 shows a plan view of the measurement grid for a single pool, and a side view of the same pool to show the measurement depths.

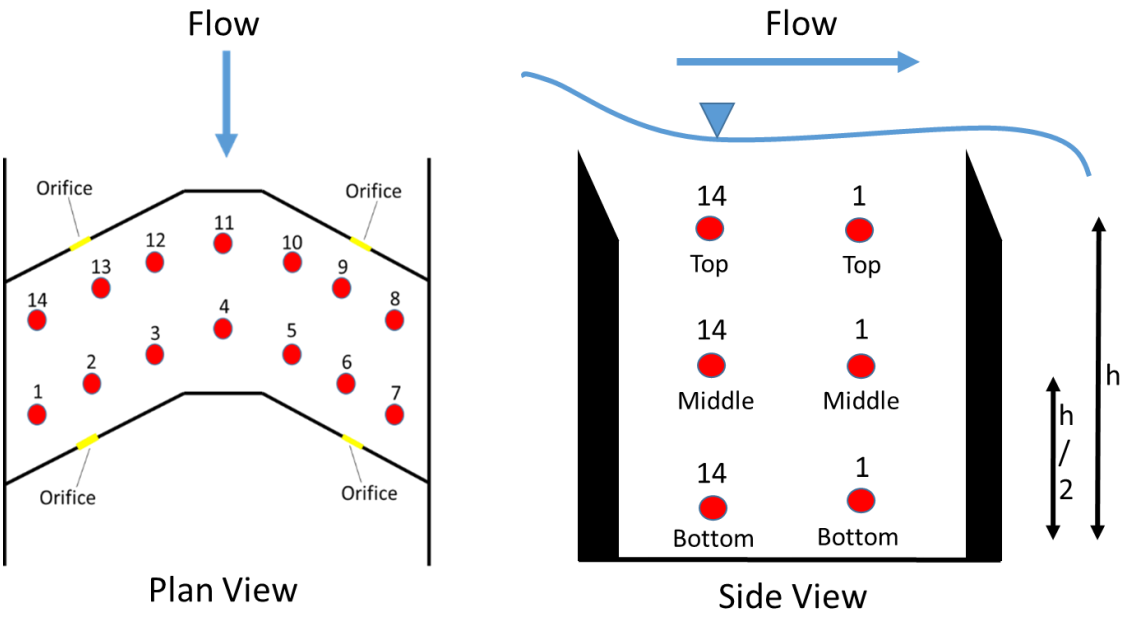

Figure 9. Plan and side view schematics of the measurement grid system for one pool.

Each data point was sampled for a minimum of 30 seconds. Points in which data did not become statistically stationary after 30 seconds were sampled for up to three minutes. A stationary time series is one whose statistical properties (e.g. mean, variance, autocorrelation, etc.) are all constant over time (Nau, 2016). Stationarity was determined by inspection during data collection, and verified in post-processing the data.

The ADV's standard internal coordinate system is such that the positive x-direction is oriented downstream in the streamwise direction and the positive y-direction is 90 degrees to the left, pointing to the left side wall. This standard orientation was used for measurements at locations 2-10, at all depths. However, given the shape of the ADV and the fishway geometry, the standard orientation could not be used at locations 1 and 11-14 because the ADV would not fit in the physical model at those locations in the standard orientation. Measurements at locations 11-14 were taken with the ADV's positive x-direction oriented upstream and positive y-direction 90 degrees to the left, pointing to the right side wall. Measurement location 1 required the ADV be oriented at a 90-degree angle, where the positive x-direction was pointed at the right side wall and the positive y-direction pointed downstream, in the streamwise direction. SonTek (2001) assures that the sensor orientation for the 2-D, side-looking ADV will perform adequately with the sensor in any orientation.

A direction test was performed in the Hydraulics Laboratory at HSU to validate the accuracy of the measurements and their conversion with the ADV oriented upstream and at a 90-degree angle. A point was measured in the flume for five minutes with the ADV pointed downstream, and the same point was measured with the ADV oriented

upstream and at a 90-degree angle for five minutes in each orientation. To correct the final velocity vectors, the vector components for points measured with the ADV oriented upstream were multiplied by negative one to change the directions of the velocity components. To correct the final velocity vectors when the ADV was oriented at a 90-degree angle at the right wall, the positive y component that is measured becomes the final positive x component, and the positive x component measured becomes the final negative y component. Table 1 shows a summary of the corrections that were made to upstream and 90-degree orientation measurements.

Table 1. Summary of ADV orientations and their directions as defined by the Cartesian coordinate system established in Figure 8.

Orientation	**x-direction**	**y-direction**
Downstream	+x	+y
Upstream	-x	-y
90 degrees right (looking downstream)	-y	+x

The direction test showed that after the directions were corrected, the measurements in all orientations produced very similar vectors which allowed the adoption of this method and validates the claim of Sontek (2001) that this ADV may be used in any orientation.

A quality assurance test was performed by re-measuring a subsample of the entire data set. All forty-two points of the middle pool of the fishway at the middle flow rate were re-measured. The recollected data was compared to the original to determine if the

measurements were consistent. Results from this test are summarized in Table 14, in the appendix. Quality was also assessed while taking measurements by monitoring the correlation coefficient. According to Sontek (2001), the correlation coefficient should be above 70% for confident and reliable measurements. For all velocity measurements for every flow rate, 81% of the measurements had a correlation coefficient above 70%. The measurements whose correlation coefficients were below 70% occurred in the same locations throughout the fishway for all flow rates. Generally, the measurement locations with correlation coefficients below 70% occurred in the centerline at all depths and in locations adjacent to orifices at the bottom depth.

Acoustic Doppler Velocimetery Data Processing

The raw velocities measured by the ADV contain four sources of error and must therefore be processed. Sampling errors occur due to the inability of the system to resolve the phase shift of the return pulse, random scatter motions within the sample volume, mean velocity shear within the sample volume, and noise inherent to the Doppler measurement technique (Voulgaris & Trowbridge, 1998). The United States Bureau of Reclamation (USBR) computer program WinADV32 (Wahl, 2004) was used to process the raw data. The program filters out data with excessive error and calculates average velocity components and magnitudes, root-mean-squared (RMS) velocity fluctuations, skewness, and kurtosis.

The skewness and kurtosis are used to assess the temporal distribution of the turbulent fluctuations of velocity around its mean. A non-zero skewness indicates the degree of temporal asymmetry of the turbulent velocity fluctuations, and a kurtosis much larger than zero is related to a peaky ADV signal created by intermittent turbulent events (Chanson, 2008). Skewness and Kurtosis were calculated as (Wahl, 2004):

$$Skewness_x = \left[\frac{n}{(n-1)(n-2)\sigma^3}\right]\left(\sum V_x^3 - \frac{3}{n}\sum V_x \sum V_x^2 + \frac{2}{n^2}\sum (V_x)^3\right) \quad [9]$$

Where: n = the number of measurements collected

σ = the standard deviation

$$Kurtosis_x = K_1\left(\sum V_x^4 - \frac{4}{n}\sum V_x \sum V_x^3 + \frac{6}{n^2}(\sum V_x)^2 \sum V_x^2 - \frac{3}{n^3}(\sum V_x)^4\right) - K_2 \quad [10]$$

Where:

$$K_1 = \frac{n(n+1)}{(n-1)(n-2)(n-3)\sigma^4}$$

$$K_2 = \frac{3(n-1)^2}{(n-2)(n-3)}$$

And: n = the number of measurements collected

σ = the standard deviation

Turbulent Kinetic Energy

TKE was calculated without the third RMS, vertical direction vector component, (w_{rms}), because the 2-D ADV was not capable of measuring it. The TKE was calculated

at each point to determine where energy was being transferred in the fishway, and how much is being dissipated. TKE was calculated as (Baki et al., 2014):

$$TKE = \frac{1}{2}({u_{rms}}^2 + {v_{rms}}^2) \quad [11]$$

To scale model TKE values to full scale, prototype TKE, the following equation was used (Calluaud et al., 2012):

$$TKE_m = \alpha TKE_p \quad [12]$$

where α is equal to model-prototype ratio of $\frac{1}{15}$.

Data Visualization

Data visualization is needed to analyze large amounts of data simultaneously. It is useful because it allows patterns and other information to more easily be recognized and quantified. Using MATLAB, a quiver plot was created to visualize the magnitude and direction of velocity vectors at each grid location. The vector arrow size is proportional to the velocity magnitude. Surface plots were created to show the distribution of turbulent kinetic energy.

The velocity vectors were also visualized in real time using an apparatus of thin steel rods at each data point with colored strings attached at the surface, middle, and bottom depths in a pool shown in plan view in Figure 25 and side view in Figure 26, in the appendix. The apparatus was built by CNRS technicians and used to observe the dominant velocity vectors and velocity fluctuations at each point and depth. These

observations were used to qualitatively confirm ADV data quality, and provide direct observations of the vertical vector component that could not be measured by the 2-D, side-looking ADV.

Identifying Migration Pathways, Fatigue, and Ascension Times

Preliminary Numerical Passage Model

A preliminary passage model was developed to determine passage efficiency through the prototype fishway for steelhead and coho salmon. Two passage routes were considered in this analysis, and were chosen based on their low streamwise velocity components and low TKE because it is generally accepted to be the most favorable conditions for passage of pacific salmonids. The first is a straight line path through the fishway that goes through points 6 and 9 on the left side of each pool. The second is a "long path" that goes through all of the points on one side of a pool, in this case the left side was chosen. The nodal path of the "long path" starts at the entrance weir close to point 6, then goes to point 6, point 9, point 10, point 5, point 6, point 7, point 8, and then to the next weir and continues this progression through the entire fishway. These two paths were chosen to estimate a range of efficiency values and not because they are necessarily likely routes. Figure 10 shows a graphic of the straight and long routes considered in the preliminary passage model. Figure 10 may be used in conjunction with Figure 9 for clarity.

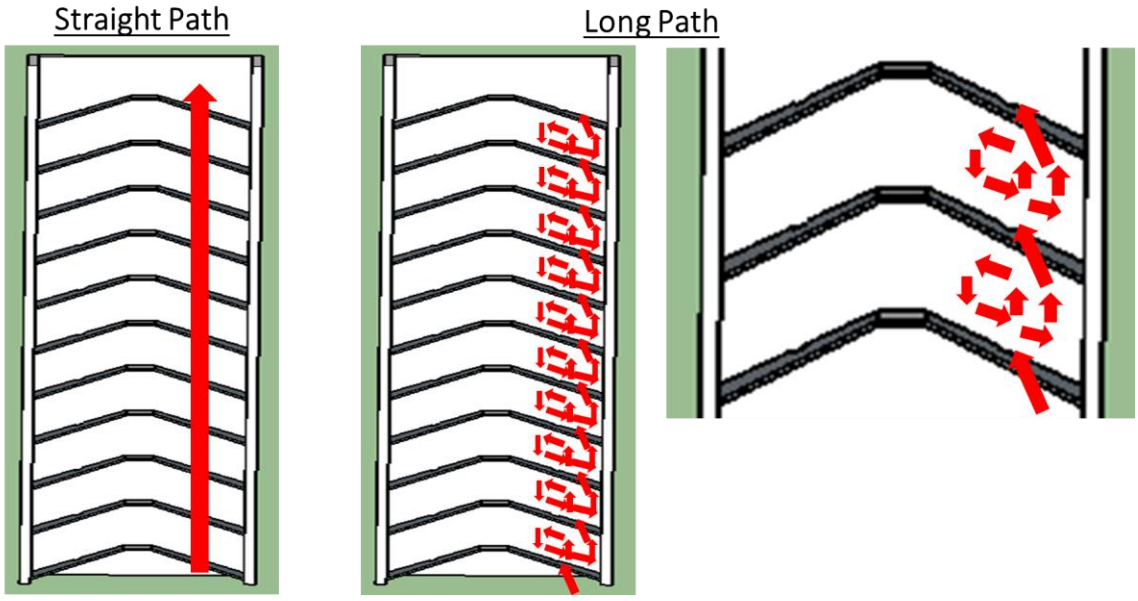

Figure 10. Plots of the straight and long pathways considered in the preliminary numerical model.

The average velocity and standard deviation of the depth-averaged velocities along these paths were calculated form the surface and middle depth stream-wise, or x-direction, velocity component. Normally distributed Monte Carlo simulations were created from the measured velocity data at the medium and high flow rate to estimate the velocity at each point along the pathway. In the long path, fish were only swimming against the stream-wise velocity component during the travel from the first three nodal movements, and then it was assumed that the fish were traveling with the flow direction. Fish were assumed to use burst swim mode to swim or jump over weirs, and prolonged swim mode while swimming in pools. If 100 F% was reached or exceeded fish were assumed to decrease swim speed at that location to a sustained swim speed of 1.0 body length per second (BL/s) to rest. Brett (1964) measured recovery from fatigue in terms of

metabolic rate for sockeye salmon and showed recovery is exponential relative to time spent resting at sustained swim speeds. Results indicate that fish may require up to 6.5 hours to fully recover; however, after 10 minutes their metabolic rate decreased by half. It was assumed that if a fish reached 100 F% they will rest for 10 minutes at that location and recover 50 F% and then continue along the pathway until the entire fishway was ascended.

Returning steelhead and coho salmon fork length measurements from Kiernan et al. (2016) and Shapovalov & Taft (1954) from three locations close to San Francisco Bay were used to calculate the average and standard deviation of the two species' fork lengths. The distribution of this data was used to sample a fork length for each fish. For the Monte Carlo simulations, fork length was assumed to be normally distributed. Using the total combined swim speeds (swimming velocity plus water velocity) and the prototype fishway distance traveled along each path, the amount of time spent in each swim mode was determined and a running total of time in each swim mode calculated for each nodal distance along each path. The times in each swim mode were converted to fatigue time for each fish in simulations of both species. The final calculation in the passage model (Eqn. 21 below) uses an equation derived by Castro-Santos (2006) for tracking a fish's percent fatigue (F%) as it swims through changing water velocities and changes in its swim modes. F% was calculated for each nodal movement and summed over the entire path length when a fish completes ascension of the fishway. One thousand steelhead and one thousand coho salmon were simulated to ascend the prototype fishway and the overall F% was calculated for each fish.

A second analysis was performed using this model to estimate the theoretical maximum length for the fishway without a single fish in the sampled ensemble reaching 100% fatigue at any point in the fishway. To determine this length, pools and weirs were added to the fishway one at a time and the simulation of one thousand steelhead and one thousand coho salmon were rerun. The maximum fishway length, where zero fish reached 100% fatigue, was considered the theoretical maximum length.

The following assumptions are used in the numerical model:

1. Fish swim continuously along two predetermined routes
2. Fish use burst swim mode to go over weirs, prolonged swim mode while swimming in pools, and a sustained swim speed of one BL/s to rest as needed
3. Sufficient depth exists throughout pools and over significant portions of the weirs under the three flow rates considered
4. All fish enter the fishway and begin ascension with 0% fatigue
5. All fish are highly motivated to migrate upstream through the fishway
6. Each time a fish reaches 100 F% it will reduce its swim speed to a sustained swim speed of 1 BL/s in that location and rest for 10 minutes. After swimming at 1 BL/s in place for 10 minutes it recovers 50% of its fatigue
7. Fish are always adjacent to an area where they can rest in sustained swim mode
8. Fork lengths of fish populations, and varying water velocities are normally distributed

9. Weir velocity was averaged over the entire cross section of plunging flow over the weir not the exact pathway location. It was calculated and not measured directly
10. Water velocities in pools were depth-averaged from middle and surface velocities measured in the scale model and scaled up

The sum of the sampled water velocities $\overrightarrow{U_w}$ and ground speed of the fish $\overrightarrow{U_g}$ yield the final swim speed of a sample fish $\overrightarrow{U_S}$. The fish swim speed was calculated as (Castro-Santos, 2005):

$$\overrightarrow{U_S} = \overrightarrow{U_g} - \overrightarrow{U_w} \quad [13]$$

Constant optimum ground speeds (U_{G-Opt}) (in body lengths per second (BL/s)) were used for the prolonged ground swim speed ($\overrightarrow{U_g}$) of each species. U_{G-Opt} was calculated using equation [15], asserted by Castro-Santos (2005), where the distance-optimizing swim speed (U_{s-opt}) is equal to the absolute value of the water velocity minus the quotient $\frac{1}{\beta}$ where β is the slope of the regression line of the log-linear relationship of fatigue time versus swim speed. Thus, U_{G-Opt} equals $\frac{1}{\beta}$.

$$U_{s-opt} = U_w - \frac{1}{\beta} \quad [14]$$

Using fatigue time versus swim speed data for steelhead and coho salmon from (Paulik & DeLacy, 1957), the optimum constant ground swim speeds (U_{G-Opt}) were calculated as follows:

Steelhead: $U_{G-Opt} = \frac{1}{0.487} = 2.05$ BL/s [15]

Coho Salmon: $U_{G-Opt} = \frac{1}{0.595} = 1.68$ BL/s [16]

Constant ground burst swim speeds were also assumed in this model. To calculate the constant ground burst swim speeds, data from Weaver (1963) were used, where steelhead and coho salmon were subjected to high water velocities of 13.4 ft/s and 15.8 ft/s and swim speeds were measured. The dominant burst swim speeds for steelhead and coho salmon were approximately 5 ft/s and 5.5 ft/s, respectively. The median fish length for the steelhead and coho salmon used by Weaver (1963) were 24 inches and 21 inches, respectively. Using those data, the burst swim speed was divided by the median fish length to calculate the constant ground burst swim speeds used in the model. For steelhead and coho salmon they were calculated as 2.5 BL/s and 3.1 BL/s, respectively. The median fish lengths from the Kiernan et al. (2016) and Shapovalov & Taft (1954) data sets were approximately 23 inches and 25 inches for steelhead and coho salmon, respectively. The median steelhead fork length from these data sets were similar to the Weaver (1963) data set, however the median coho salmon fork length was higher by approximately 4 inches.

Fatigue times were calculated separately for prolonged and burst swim modes. Fatigue times for prolonged swim mode were calculated by solving the regression equation determined from plotting the fatigue time (T_{mean}) versus swim speed (U_s) data from Paulik and Delacy (1958), for steelhead and coho salmon. Those equations are:

Steelhead: $\ln(T_{mean}) = -0.487U_s + 6.447$ [17]

Coho Salmon: $\ln(T_{mean}) = -0.595U_s + 6.600$ [18]

Fatigue times for burst swim mode were calculated by solving equations presented by Hunter and Mayor (1986) for time. They fit a power function to describe the swim speed (U_s) as a function of fish length (L) and time to fatigue (T). The burst swim speed equations for coho salmon and steelhead used were:

Coho Salmon Burst Swim Speed

$$U_s = 13.3L^{0.52}T^{0.65} \quad [19]$$

Steelhead Burst Swim Speed

$$U_s = 12.3L^{0.62}T^{0.51} \quad [20]$$

To calculate percent fatigue (F%) of a fish while it swims at variable speeds requires summing the amount of time swum at each speed (t_{U_s}) divided by the fatigue time associated with that swim speed (T_{U_s}). Equation [22] is the equation used to calculate F% (Castro-Santos, 2006):

$$F\% = 100\times\sum\frac{t_{U_s}}{T_{U_s}} = 100\times\sum\left(\frac{t_{U_sburst}}{T_{U_sburst}} + \frac{t_{U_sprolonged}}{T_{U_sprolonged}}\right) \quad [21]$$

The Data Tables function in Microsoft Excel was used to solve the percent fatigue and travel time from ascending the entire prototype fishway for one thousand randomly sampled steelhead and one thousand randomly sampled coho salmon. These simulations were performed on the prototype fishway for two routes, the straight path and the long path. These simulations also considered two flow rates, the medium and high flow rate. The last simulations extended the length of the prototype fishway to its theoretical maximum length, holding width constant at 30 feet, where no fish reach 100% fatigue.

Simulations for the extended fishways were also run at the medium and high flow rates and the two different routes. There are sixteen total scenarios that were created from the eight combinations of flow, pathway, and fishway length for the two species of fish, hence referred to as “passage scenarios”. The scenarios are labeled such that the first letter is an “M” or “H” and represents the medium and high flow rate, respectively. The second letter is an “S” or “L” and represents the straight and long pathways, respectively. The third letter is a “D” or an “E” and represents the design fishway length of 144 feet or the calculated theoretical maximum extension length, respectively. Lastly, the final two letters in the scenario labels are “St” or “Co” and represent steelhead and coho salmon, respectively. Table 2 summarizes the fish species, flow rate, pathway, and fishway length used in each of the sixteen total scenarios considered. The final product of this model quantifies the passage efficiency of the simulated fish for each scenario in terms of passage success, time elapsed, and percent fatigue.

Table 2. Summary of the fish species, flow rate, pathway, and fishway length used for each of the sixteen scenarios run in the preliminary numerical model.

Scenario	Species	Flow Rate	Pathway	Fishway Length
MSDSt	Steelhead	Medium	Straight	Design
MLDSt	Steelhead	Medium	Long	Design
MSESt	Steelhead	Medium	Straight	Extended
MLESt	Steelhead	Medium	Long	Extended
HSDSt	Steelhead	High	Straight	Design
HLDSt	Steelhead	High	Long	Design
HSESt	Steelhead	High	Straight	Extended
HLESt	Steelhead	High	Long	Extended
MSDCo	Coho	Medium	Straight	Design
MLDCo	Coho	Medium	Long	Design
MSECo	Coho	Medium	Straight	Extended
MLECo	Coho	Medium	Long	Extended
HSDCo	Coho	High	Straight	Design
HLDCo	Coho	High	Long	Design
HSECo	Coho	High	Straight	Extended
HLECo	Coho	High	Long	Extended

RESULTS

Introduction

This section presents the results from testing the physical model and passage efficiency analysis from the preliminary passage model. The first section presents the scaled up, prototype velocity vectors and TKE values at each of the three flow rates. The next section presents the results from running the Monte Carlo simulations through the prototype fishway to estimate passage efficiency for the scenarios described in the methods section, and then presents the results from extension of the fishway and ascension times for all scenarios. Results from the flume V-notch calibration are included in the appendix section.

Velocities and Turbulent Kinetic Energy

High Flow

Figure 11 shows three plots with the point velocity vectors for the high flow rate at the surface, middle, and bottom depth. The velocity vectors on the sides of the pools appear to experience a combination of lateral, elliptical rotations as well as longitudinal rotations (figure 11). There are multiple eddies within each pool of the fishway with two primary axes of rotation. There is one large eddy in the longitudinal direction and one in the lateral direction. However, at the high flow rate, along the centerline there appears to

be only one dominant large eddy in the longitudinal direction as evidenced by velocity vectors pointed downstream near the surface of each pool and in the upstream direction at the bottom depth of each pool shown in Figure 11.

The sides of the pools have a lateral eddy indicating they have a transitional flow regime with angled flow vectors with one exception. The area that is closest to the side walls appears to exhibit a plunging flow, also with angled flow vectors. The flow vectors directly adjacent to the side walls are pointed upstream at all depths and are angled slightly towards the side wall on the downstream ends of the pools and slightly away from the side walls at the upstream ends of the pools because of the geometry of the weirs that create the large lateral eddies which dominate the overall directions of flow. These large eddies were maintained in each pool by the weir geometry and constant flow rate and experience turbulent fluctuations.

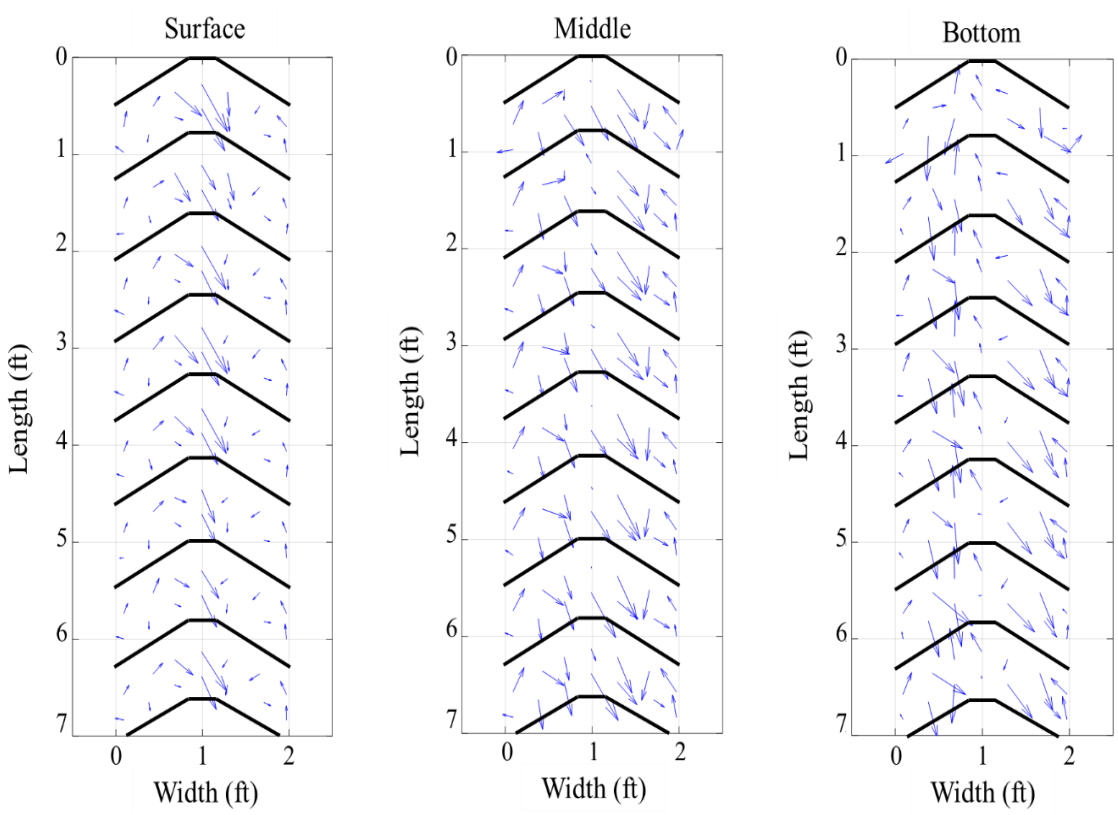

Figure 11. Plots of prototype velocity vectors at surface, middle, and bottom depths for high flow rate (181 cfs).

At the surface of the pools, the highest velocities are concentrated along the centerline. The maximum velocity measured was in the centerline, at the surface and is equivalent to a prototype velocity of 9.10 ft/s. On the pool sides, the lower velocities rotate as predictable eddies. At the pool surface, the eddies on the right side of the pools spin clockwise and the eddies on the left side of the pools spin counter-clockwise when looking downstream. At the fishway sidewalls the direction of flow was noted to be going directly upstream and this was confirmed with the string apparatus. Using the string apparatus, conventional vertical rotation eddies in the longitudinal direction for

streaming and plunging flow were also confirmed to be present in the pools. Table 3 shows the average, maximum and minimum velocities in the fishway for the surface, middle, and bottom depths, and separated by centerline or side pools.

Table 3. Summary of average, maximum, and minimum prototype velocities separated by depth and area in fishway, for high flow rate (181 cfs).

	Surface - Centerline	**Surface - Sides of Pools**	**Middle - Centerline**	**Middle - Sides of Pools**	**Bottom - Centerline**	**Bottom - Sides of Pools**
Average Prototype Velocity (ft/s)	6.81	2.03	1.53	1.89	1.15	2.19
Maximum Prototype Velocity (ft/s)	9.10	6.30	4.09	3.73	1.99	4.56
Minimum Prototype Velocity (ft/s)	4.73	0.77	0.06	0.51	0.19	0.37

Under the high flow condition at the middle depth, the velocity in the centerline at point 11 is very small and changing direction between upstream and downstream, and at point 4 the velocity was relatively high at 4.09 ft/s. At the middle depth, the eddies at the sides of the pools are spinning in the same vortical, rotational direction and at nearly the same velocity, but slightly slower. Similar to the surface, the flow near the sidewalls are going directly upstream and conventional eddies in the longitudinal direction were present. TKE values, similarly to the surface, were directly proportional to the velocity magnitudes.

Under the high flow condition, at the bottom depth, the centerline velocities are in the upstream direction. The eddies maintain their rotational direction with the exception of the points that were located at the orifices. Those points were sometimes dominated by the direction and magnitude of the jet exiting the orifice. The maximum velocity at the bottom depth was in the centerline and is equivalent to a prototype velocity of 1.99 ft/s.

The plots in Figure 11 also revealed that the velocity vectors were pointed slightly to the left when looking downstream. There was a bias to the left side due to a slight tilt in the flume and not due to the weir geometry.

The TKE values are distributed in a similar pattern to the velocity magnitudes, e.g. the location with the highest velocity has the highest TKE and the location with the lowest velocity has the lowest TKE. The average, maximum, and minimum TKE values in all pools are summarized in

Table 4 and a visualization of the TKE can be seen in Figure 12. The highest TKE values were focused at the centerline of the fishway, with the highest TKE values occurring at the surface and decreasing with depth. The highest TKE is equivalent to a prototype TKE value of 1.27 m^2/s^2. The sides of the pools contained significantly less TKE, with an average TKE value in the sides of the pools of 0.08 m^2/s^2. The bottom depth along the centerline exhibited similar levels of TKE as the sides of the pools.

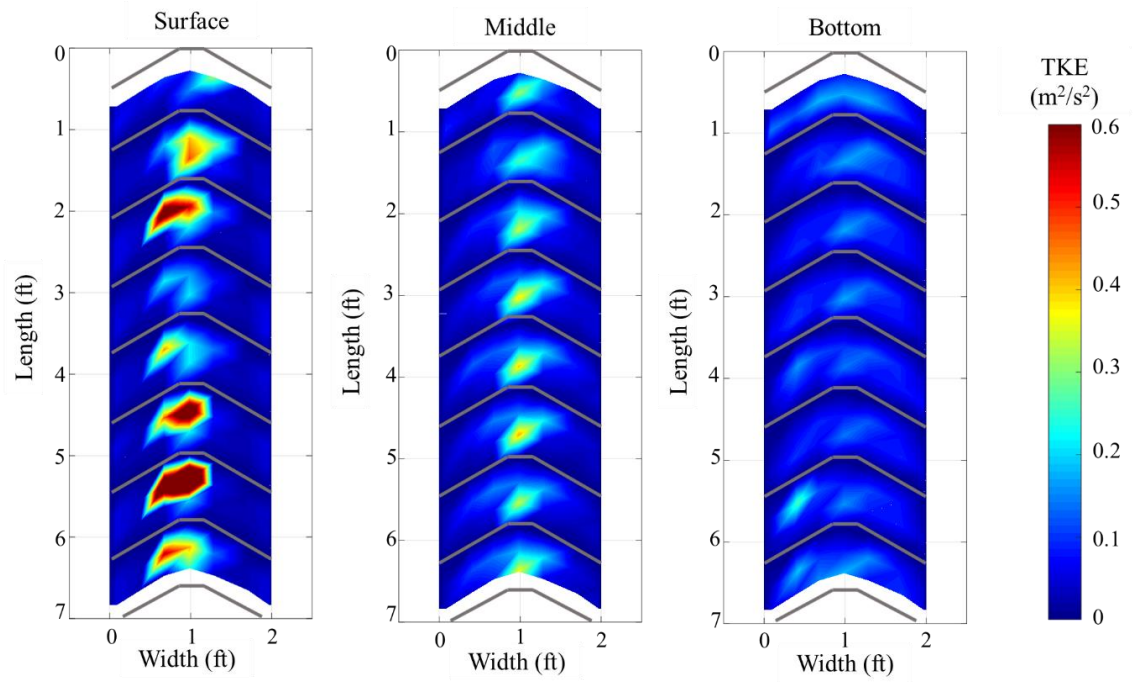

Figure 12. Plots of the distribution of prototype TKE levels for high flow rate (181 cfs).

Table 4. Summary of average, maximum, and minimum prototype TKE values separated by depth and area in fishway, for high flow rate (181 cfs).

	Surface - Centerline	**Surface - Sides of Pools**	**Middle - Centerline**	**Middle - Sides of Pools**	**Bottom - Centerline**	**Bottom - Sides of Pools**
Average Prototype TKE (m^2/s^2)	0.37	0.08	0.25	0.07	0.12	0.08
Maximum Prototype TKE (m^2/s^2)	1.26	0.91	0.42	0.24	0.18	0.27
Minimum Prototype TKE (m^2/s^2)	0.08	0.01	0.07	0.02	0.08	0.01

The skewness and kurtosis values measured at each point and in the x and y direction show that at all depths the majority of the measurements had a non-zero skew, and a kurtosis value less than zero. This suggests that the turbulent fluctuations are asymmetrical but mostly continuous (Chanson, 2008). The number of 2-D zero and non-zero skewness, and positive and negative kurtosis measurements for each depth, for the high flow rate (181 cfs) are summarized in **Error! Not a valid bookmark self-reference.**.

Table 5. Number of 2-D zero and non-zero skewness, and positive and negative kurtosis measurements separated by depth, for high flow rate (181 cfs).

	Zero Skew	**Non-Zero Skew**	**Kurtosis > 0**	**Kurtosis < 0**
Surface	19	205	58	166
Middle	25	199	35	189
Bottom	16	208	35	189

Medium Flow

The medium flow rate point velocities did not show clear streaming flow conditions, suggesting this flow rate contains only plunging and transitional flow through the fishway. Figure 13 shows three plots with the point velocity vectors for the medium flow rate at the surface, middle, and bottom depth. Visual observation of the flow regime along the fishway centerline appears to most resemble streaming flow from but vectors at the bottom and middle depths of each pool in the centerline suggest that it is a transitional flow regime because velocity vectors are pointed downstream at these locations.

Under the medium flow rate, at the surface of the pools, the fastest velocities measured were along the centerline, with slower velocities rotating predictably at the sides of the pool. The maximum velocity measured, 8.34 ft/s, was in the centerline at the surface. The average, maximum, minimum velocity values are summarized in Table 6.

Under the medium flow rate, at the middle depth, point 11 has a very small velocity magnitude that was observed to change direction from upstream to downstream. At the bottom depth and in the centerline, point 11 has a velocity vector in the upstream direction and point 4 has a vector in the downstream direction. The eddies maintain their rotational direction with the exception of the points located at the orifices. Those points were sometimes dominated by the direction and magnitude of the jet from the orifice. At the middle depth the centerline velocities remain the highest throughout each of the pools with slightly lower velocities at the sides of the pools.

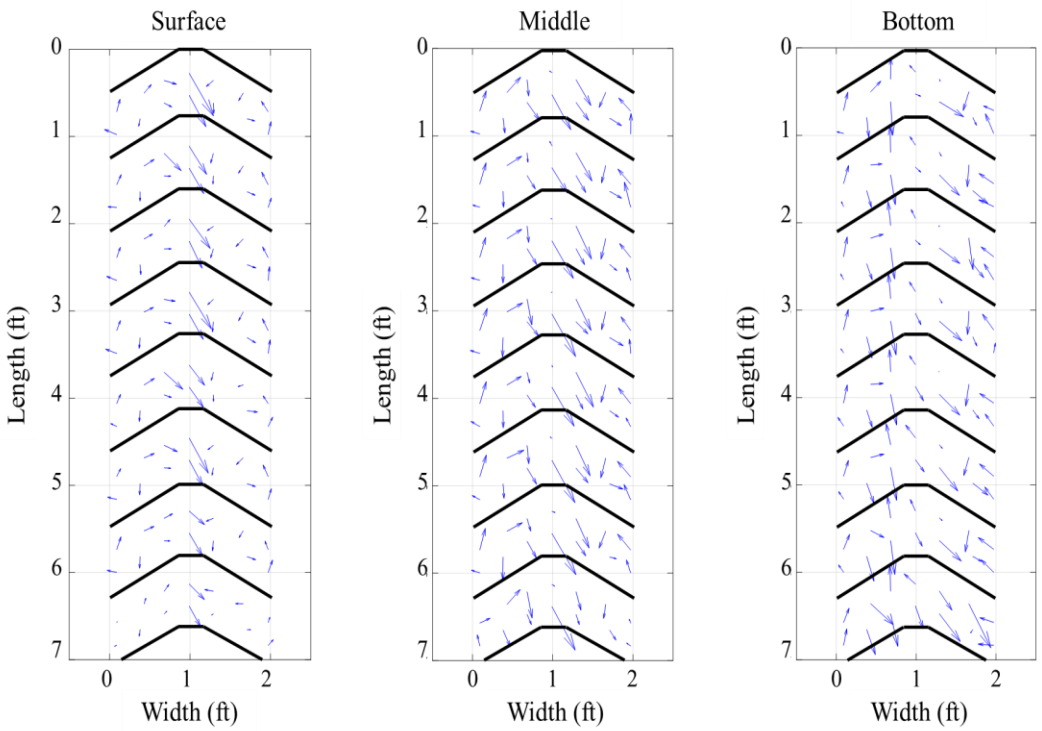

Figure 13. Plots of velocity vectors at surface, middle, and bottom depths for medium flow rate (144 cfs).

Table 6. Summary of average, maximum, and minimum prototype velocities separated by depths and area in fishway, for medium flow rate (144 cfs).

	Surface - Centerline	**Surface - Sides of Pools**	**Middle - Centerline**	**Middle - Sides of Pools**	**Bottom - Centerline**	**Bottom - Sides of Pools**
Average Prototype Velocity (ft/s)	5.30	1.66	2.21	1.68	1.32	2.01
Maximum Prototype Velocity (ft/s)	8.34	4.38	4.69	3.69	2.53	5.25
Minimum Prototype Velocity (ft/s)	3.57	0.16	0.07	0.37	0.65	0.04

The TKE was focused along the centerline of the fishway, with the highest TKE values occurring at the surface and decreasing with depth, as shown in Figure 14. The highest TKE value measured was 1.00 m^2/s^2. The sides of the pools contained significantly lower TKE, with an average TKE value of 0.05 m^2/s^2. The bottom depth of the centerline exhibited similar levels of TKE as the sides of the pools. A summary of the average, maximum, and minimum TKE values for the medium flow rate is provided in

Table 7.

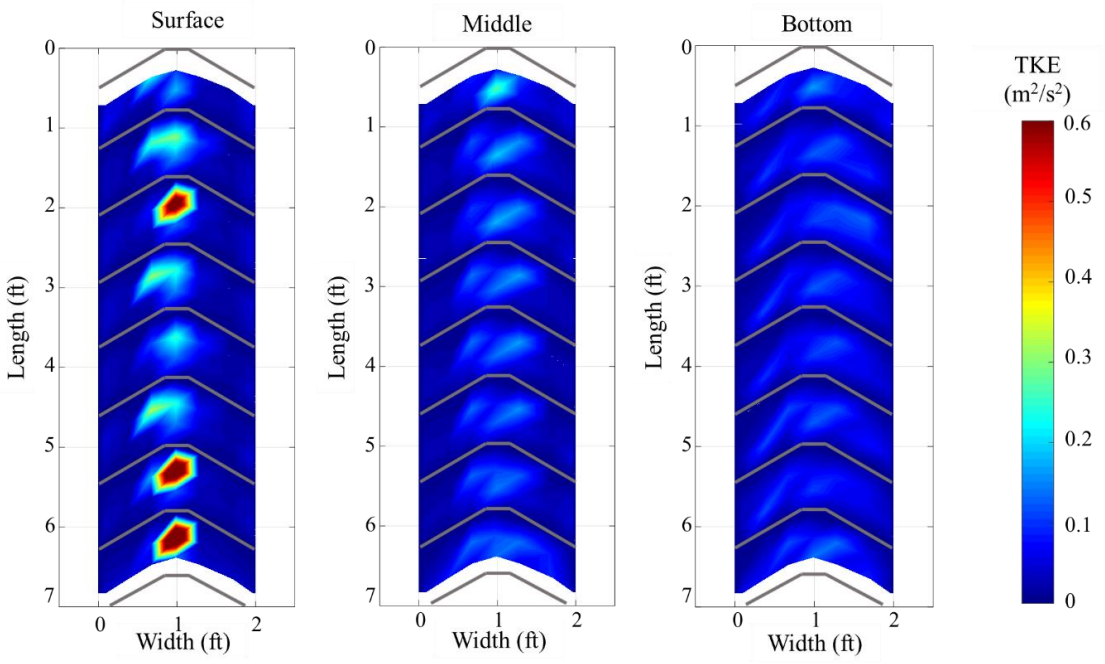

Figure 14. Plots of the distribution of prototype TKE levels for medium flow rate (144 cfs).

Table 7. Summary of average, maximum, and minimum prototype TKE values separated by depth and area in fishway, for medium flow rate (144 cfs).

	Surface - Centerline	Surface - Sides of Pools	Middle - Centerline	Middle - Sides of Pools	Bottom - Centerline	Bottom - Sides of Pools
Average Prototype TKE (m^2/s^2)	0.33	0.04	0.12	0.05	0.09	0.06
Maximum Prototype TKE (m^2/s^2)	1.00	0.33	0.28	0.17	0.16	0.14
Minimum Prototype TKE (m^2/s^2)	0.10	0.01	0.06	0.01	0.05	0.01

The number of 2-D skewness and kurtosis measurements separated by zero and non-zero, and greater than and less than zero, respectively are shown in Table 8. These results were similar to the high flow rate, where most of the skewness measurements were non-zero, and most of the kurtosis measurements were less than zero.

Table 8. Number of 2-D skewness and kurtosis measurements separated by depth, for medium flow rate (144 cfs).

	Zero Skew	Non-Zero Skew	Kurtosis > 0	Kurtosis < 0
Surface	17	207	58	166
Middle	19	205	59	165
Bottom	17	207	60	164

Low Flow

Under the low flow conditions, the flow regime along the fishway centerline exhibits transitional flow. The area of flow closest to the side walls appears to exhibit a plunging flow regime with angled flow vectors as described in the high flow results

section. Figure 15 shows three plots with the point velocity vectors for the high flow rate at the surface, middle, and bottom depth.

Under the low flow rate, at the surface of the pools, the largest velocity vectors were in the centerline of the pools, and the lowest velocities were at the sides of the pools. The highest velocity recorded was in the centerline, at the surface, and measured 5.91 ft/s. The average, maximum, and minimum velocity values are summarized in Table 9.

Under the low flow rate, at the middle depth, the centerline also contained the largest velocities. In the pool sides, the lateral eddies dominated the flow directions in the same directions as the other two flow rates. The velocity magnitudes at the middle depth were close together throughout the pools. The mean velocity under the low flow rate, at the middle depth in the centerline and on the pool sides are 2.53 ft/s and 2.72 ft/s, respectively.

At the bottom depth, the fastest velocities in general were measured along the centerline, with mean velocities around 2.72 ft/s. The velocities at the pool sides were smaller with mean equivalent prototype velocity of 1.05 ft/s. At the bottom depth, the vectors near the orifices are prominent and the vectors adjacent to the orifices on the downstream end of the pools (i.e. points 1 and 7) were observed to feed into the jet carrying the water through the orifices.

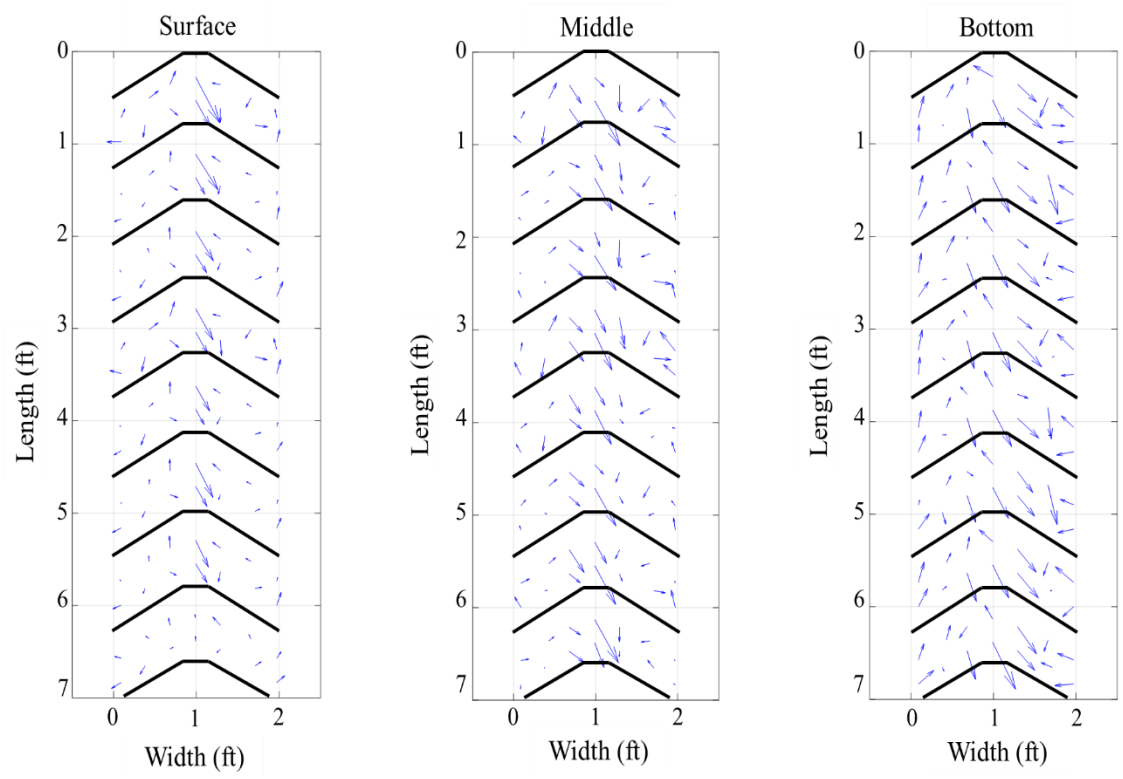

Figure 15. Plots of velocity vectors at surface, middle, and bottom depths for low flow rate (107 cfs).

Table 9. Summary of average, maximum, and minimum prototype velocities separated by depths and area in fishway, for low flow rate (107 cfs).

	Surface - Centerline	**Surface - Sides of Pools**	**Middle - Centerline**	**Middle - Sides of Pools**	**Bottom - Centerline**	**Bottom - Sides of Pools**
Average Prototype Velocity (ft/s)	3.04	0.99	2.53	1.00	2.72	1.05
Maximum Prototype Velocity (ft/s)	5.91	1.81	4.21	4.01	4.91	3.81
Minimum Prototype Velocity (ft/s)	0.35	0.14	1.06	0.05	1.49	0.11

The highest TKE values were concentrated along the centerline and were lower at the sides of the pools. The TKE values at the sides of the pools were similar at all depths. A visualization of the TKE values at the three depths is shown in Figure 16. The average, maximum, and minimum TKE values, separated into centerline and side of pool measurements, are summarized in Table 10.

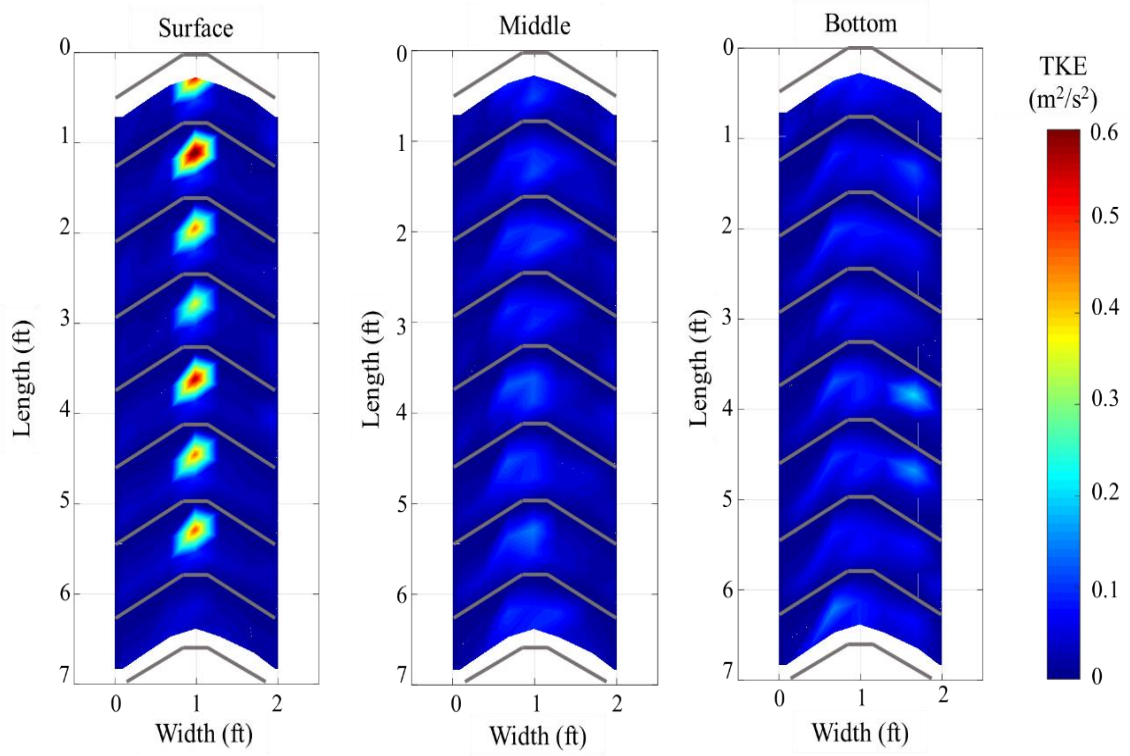

Figure 16. Plots of the distribution of prototype TKE levels for low flow rate (107 cfs).

Table 10. Number of average, maximum, and minimum prototype TKE values separated by depth and area in fishway, for low flow rate (107 cfs).

	Surface - Centerline	**Surface - Sides of Pools**	**Middle - Centerline**	**Middle - Sides of Pools**	**Bottom - Centerline**	**Bottom - Sides of Pools**
Average Prototype TKE (m^2/s^2)	0.27	0.02	0.10	0.04	0.08	0.04
Maximum Prototype TKE (m^2/s^2)	0.67	0.06	0.14	0.12	0.09	0.20
Minimum Prototype TKE (m^2/s^2)	0.03	0.01	0.07	0.01	0.05	0.00

The number of 2-D skewness and kurtosis measurements separated by zero and non-zero, and greater than and less than zero, respectively are shown in Table 11. Like the other flow rates, the skewness and kurtosis measurements were consistent at the low flow rate, where most of the skewness measurements were non-zero, and most of the kurtosis measurements were less than zero, which suggests that the turbulent fluctuations are asymmetrical but mostly continuous (Chanson, 2008).

Table 11. Summary of 2-D skewness and kurtosis measurements separated by depth, for low flow rate (107 cfs).

	Zero Skew	**Non-Zero Skew**	**Kurtosis > 0**	**Kurtosis < 0**
Surface	23	201	50	174
Middle	26	198	40	184
Bottom	20	204	51	173

Percent Fatigue and Ascension Times

Percent Fatigue (F%)

The mean F% for steelhead for the design fishway length scenarios ranged from 41.2-47.7 F% and for coho salmon ranged from 44.7-53.5 F%. For the eight passage scenarios at the design fishway length the mean F% was 3.5-5.8 F% higher for coho salmon than steelhead. The median F% values for all scenarios at the design fishway length for both species were close in value to the mean F% values but slightly lower in every scenario. The standard deviation of all eight passage scenarios at the design fishway length ranged from 3.5-4.5 F% for steelhead and 1.9- 2.8 F% for coho salmon.

The minimum F% for the eight passage at the design fishway length scenarios ranged from 34.3-40.6 F% for steelhead and 39.7-48.2 F% for coho salmon. The maximum F% for all eight passage scenarios at the design fishway length ranged from 75.2-88.8 F% for steelhead and 53.2-69.8 F% for coho salmon. Table 12 summarizes the mean, median, standard deviation, minimum and maximum F% for all eight passage scenarios evaluated for the two species and Figure 17 shows a bar graph of the mean F% for all eight passage scenarios at design fishway length for the two species.

Table 12. Summary of basic descriptive statistics of percent fatigue for one hundred replicates of one thousand simulated fish and all passage scenarios.

Scenario	Mean	Median	Standard Deviation	Minimum	Maximum
MSDSt	41.2	40.5	3.5	34.3	75.2
MLDSt	47.3	46.4	4.2	40.5	79.7
MSESt	64.9	63.9	5.4	54.4	95.1
MLESt	61.0	59.9	5.2	52.2	93.0
HSDSt	42.0	41.3	4.0	35.1	75.7
HLDSt	47.7	46.8	4.5	40.6	88.8
HSESt	58.4	57.8	5.0	48.4	86.5
HLESt	61.7	60.3	5.8	53	94.9
MSDCo	44.7	44.5	1.9	39.7	53.2
MLDCo	52.9	52.5	2.7	47.0	66.0
MSECo	70.8	70.4	3.0	64.1	84.4
MLECo	68.5	67.8	3.5	62.1	85.5
HSDCo	46.3	45.9	2.5	40.4	57.2
HLDCo	53.5	53.0	2.8	48.2	69.8
HSECo	72.9	72.4	3.6	64.6	88.0
HLECo	69.2	68.7	3.7	61.7	87.6

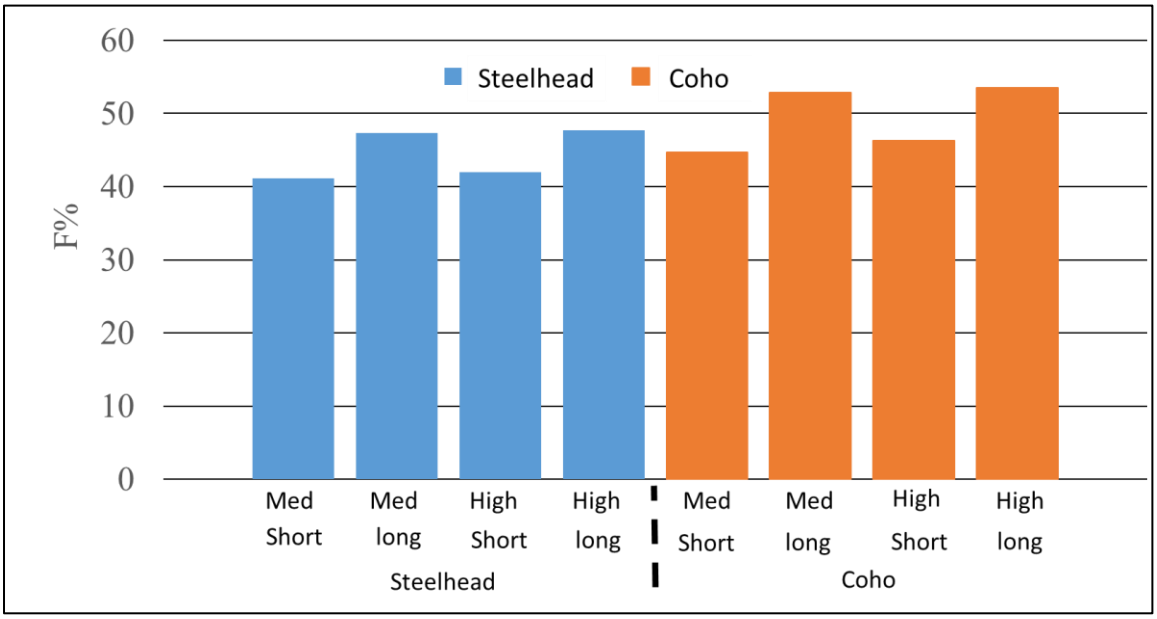

Figure 17. Bar graph of mean percent fatigue for 100 replicates of 1000 fish for each passage scenario at the design fishway length for both steelhead and coho salmon.

For the eight scenarios where the fishway length was extended to its theoretical maximum the mean F% for steelhead for the extended fishway length scenarios ranged from 58.4-64.9 F% for steelhead and 68.5-72.9 F% for coho salmon. The median F% values were slightly lower for each one of these scenarios. The standard deviation of all eight scenarios with extended fishway lengths ranged from 5.0-5.8 for steelhead and 3.0-3.7 for coho salmon. The minimum F% for the eight passage at the extended fishway lengths scenarios ranged from 48.4-54.4 F% for steelhead and 61.7-64.6 F% for coho salmon. The maximum F% for all eight passage scenarios at the extended fishway lengths ranged from 86.5-95.1 F% for steelhead and 84.4-88.0 F% for coho salmon.

The lowest F% for both steelhead and coho salmon occurred under passage scenarios with a straight pathway at the designed fishway length. This makes sense

because these scenarios minimized the amount of travel distance. Similarly, the highest F% for both steelhead and coho salmon occurred under passage scenarios with a long pathway at an extended fishway length. Differences in F% between the medium and high flow rate for the design fishway length ranged from 0.4-1.6 F% for both steelhead and coho salmon. The difference in F% between the medium and high flow rates when all other factors were held equal was minimal. While differences in F% between the straight and long pathways for the design fishway length ranged from 5.7-8.2 F% for both steelhead and coho salmon. The difference in F% between the straight and long pathway were larger.

Figures 18-21 show the raw outputs from the preliminary passage model in terms of F% for the sampled fish fork lengths for 1000 fish for four scenarios. Figures 18-21 show the general trends of the distributions for all of the scenarios. The raw output plots for the twelve remaining scenarios are provided in the appendix section. Figure 18 shows the F% for 1000 steelhead completing ascension along the straight pathway under the high flow rate. When comparing Figure 18 to Figure 19 which is the same passage scenario only for coho salmon instead of steelhead, results indicate that coho salmon are incurring more F% on average, but there is much more variability with steelhead. Figure 20 shows the F% values for 1000 steelhead from ascending up the prototype fishway along the long pathway under the high flow rate. When comparing Figure 20 to Figure 21 which shows the results for the same passage scenario as Figure 20 only for coho salmon, results indicate the long pathway increases F% significantly. Similar to Figure 18 and

Figure 19 there is more variability with steelhead while on average coho salmon are incurring more F%.

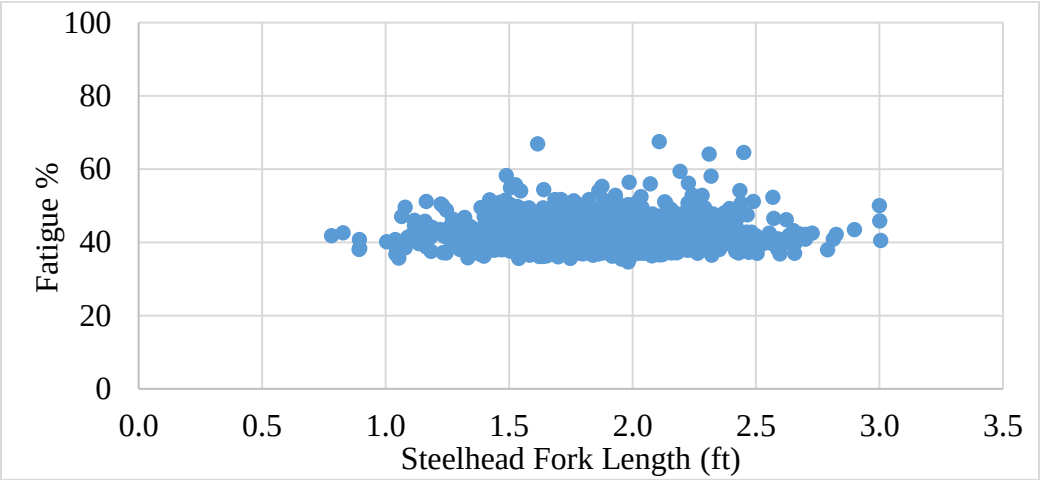

Figure 18. Plot of one thousand simulated Steelhead and their percent fatigue from completing the ascension of the prototype fishway on the straight pathway for the high flow rate.

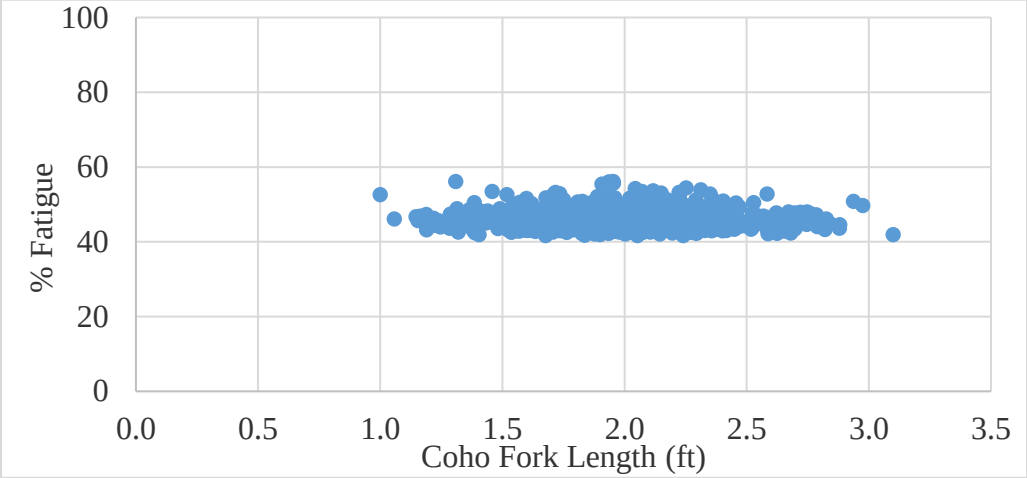

Figure 19. Plot of one thousand simulated Coho salmon and their percent fatigue from completing the ascension of the prototype fishway on the straight pathway for the high flow rate.

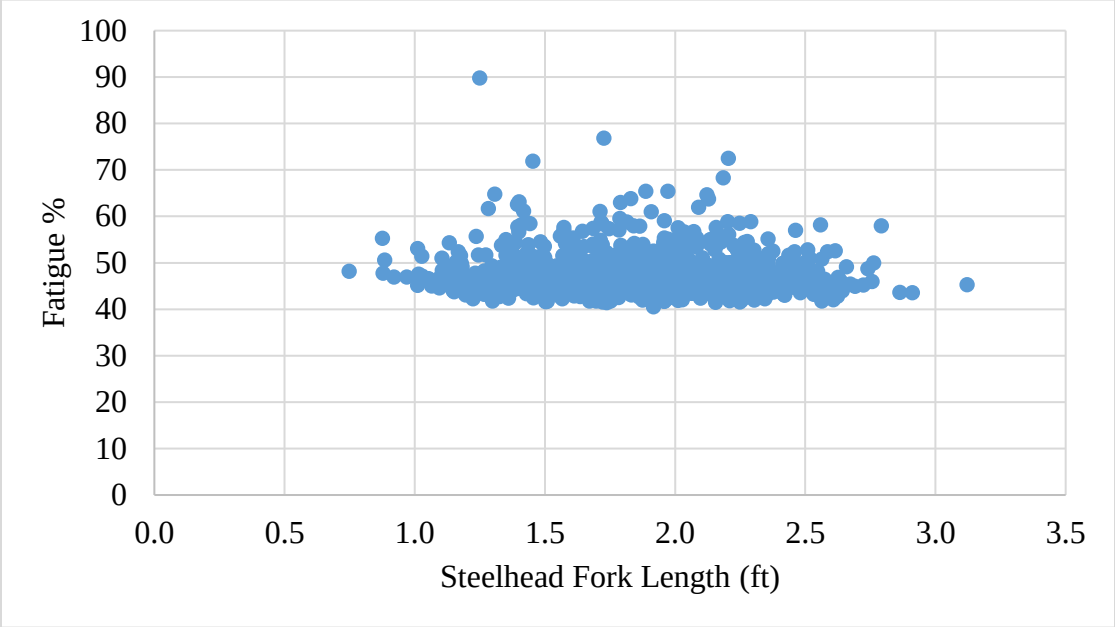

Figure 20. Plot of one thousand simulated Steelhead and their percent fatigue from completing the ascension of the prototype fishway on the long pathway for the high flow rate.

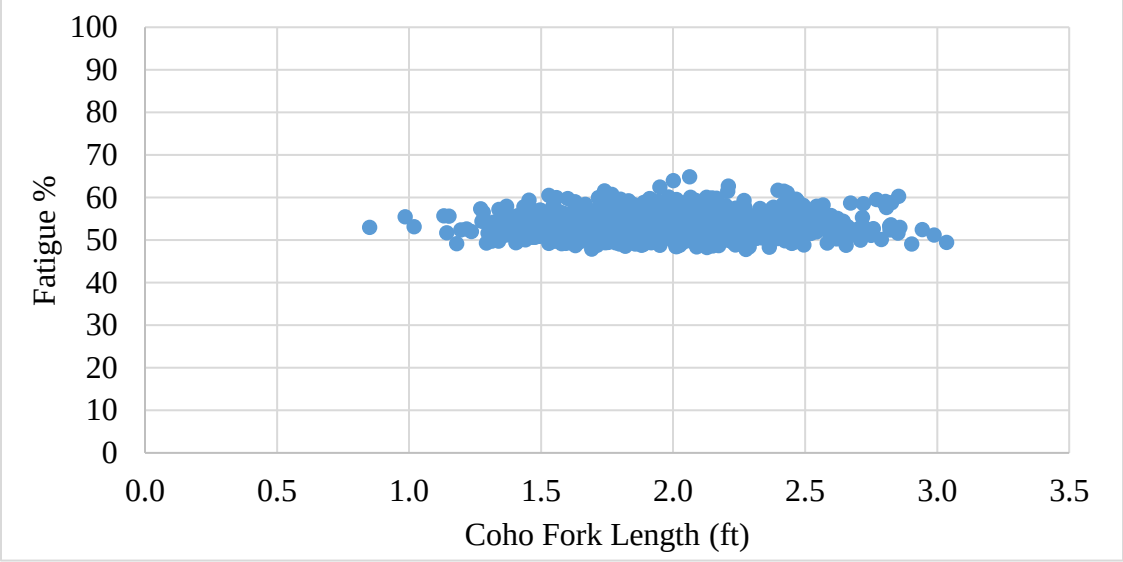

Figure 21. Plot of one thousand simulated Coho salmon and their percent fatigue from completing the ascension of the prototype fishway on the long pathway for the high flow rate.

Fishway Extension

For eight scenarios the fishway length was extended to the theoretical maximum length where a single fish within a sampled distribution was estimated to reach or exceed 100 percent fatigue (100 F%). Pool and weir sets were added to extend the fishway and 100 replications of each 1000 fish simulation were performed to verify that no fish had reached or exceeded 100 F%. As soon as an addition of a pool and weir set caused at least one fish in the run of 1000 fish to reach or exceed 100 F% that length was determined to be the maximum. However, this produced variable theoretical maximum lengths because some simulations resulted in 1 to 10 fish reaching or exceeding 100 F%, while others had over 500 fish reach or exceed 100 F%. The number of additional pool and weir sets added to the length of the fishway ranged from 3 (37.5 feet) to 6 (75 feet). Three sets of pools and weirs were found to be able to be added to scenarios MLESt, MLECo, HLESt, and HLECo, which all use the long pathway. Four sets of pools and weirs could be added to scenario HSESt, and six sets of pools and weirs to scenarios MSESt, MSECo, and HSECo, which were under the medium flow rate. These theoretical maximum lengths continue to assume that all fish only utilize the two predetermined migration pathways.

Ascension Times

Similar to the F%, the mean estimated times to ascend the prototype fishway were longer under all passage scenarios for coho salmon than steelhead. The mean ascension times for steelhead under all passage scenarios at the design fishway length ranged from 43.9-73.0 seconds for steelhead compared to 51.3-88.0 seconds for coho salmon, and the

median ascension times were very similar. The standard deviation of ascension times for the passage scenarios at the design fishway length ranged from 1.1-2.5 for steelhead and 1.2-2.5 for coho salmon. The minimum ascension times for the design fishway length ranged from 32.6-66.5 seconds for steelhead and 39.6-83.1 seconds coho salmon. While the maximum ascension times for the design fishway length ranged from 49.4-75.7 seconds for steelhead and 57.3-91.1 seconds for coho salmon.

The range of fishway extension lengths ranged from 37.5 to 75 feet. The mean ascension times for steelhead under all passage scenarios at the various extended fishway lengths ranged from 61.2-94.8 seconds for steelhead compared to 92.1-114.3 seconds for coho salmon. The median ascension times for the extended fishway lengths was greater than the mean for all scenarios by 0.2-0.6 seconds. The standard deviation of ascension times for the passage scenarios at the extended fishway lengths ranged from 1.4-3.6 for steelhead and 1.4-4.1 for coho salmon. The minimum ascension times for the extended fishway lengths ranged from 42.9-89.0 seconds for steelhead and 62.8-107.6 seconds coho salmon. While the maximum ascension times for the extended fishway lengths ranged from 69.1-98.0 seconds for steelhead and 93.1-119.1 seconds for coho salmon. Table 13 summarizes the mean, median, standard deviation, minimum and maximum ascension times for all sixteen scenarios.

Table 13. Summary of ascension time descriptive statistics for one thousand simulated fish and all passage scenarios.

Scenario	Mean	Median	Standard Deviation	Minimum	Maximum
MSDSt	48.8	49.0	2.1	32.6	53.4
MLDSt	73.0	73.2	1.1	66.5	75.7
MSESt	78.1	78.7	3.3	53.8	84.5
MLESt	94.8	95.0	1.4	89.0	98.0
HSDSt	43.9	44.1	2.5	30.8	49.4
HLDSt	71.8	71.9	1.2	63.7	74.6
HSESt	61.2	61.7	3.6	42.9	69.1
HLESt	93.2	93.4	1.6	84.1	96.5
MSDCo	57.7	57.9	2.1	46.4	62.8
MLDCo	88.0	88.2	1.2	83.1	91.1
MSECo	92.1	92.5	3.2	75.3	100.1
MLECo	114.3	114.5	1.4	107.6	119.1
HSDCo	51.3	51.7	2.5	39.6	57.3
HLDCo	86.4	86.5	1.2	80.9	89.3
HSECo	81.9	82.3	4.1	62.8	93.1
HLECo	112.3	112.4	1.6	101.2	116.1

DISCUSSION

Introduction

The discussion section explains the meaning of the results and their implications. This section is presented in the same order as the results section by first describing the direct measurements made during the flume experiments, and then explaining the simulations of fish passage through the design and extended length fishways.

Velocities and Turbulent Kinetic Energy

High Flow

From Table 3 and

Table 4 the highest velocities and TKE values under the high flow rate are concentrated along the centerline of the fishway at the surface. Figure 11 shows the velocity vectors in the centerline are pointing downstream at the surface and upstream at the bottom and decrease in magnitude in the downstream direction. Velocity magnitudes in the centerline range from 9.1 ft/s near the top of the fishway in the in the third pool from the top to 8.0 ft/s in the bottom pool of the fishway, closest to the entrance weir, which may hinder attraction flow downstream of the entrance weir. Figure 11 also shows that the sides of the pools are dominated by lateral eddies at all depths but also maintain a longitudinal eddy. From Table 3 the velocities at the sides of the pools are much lower in magnitude then in the centerline making it optimal for fish passage. The lowest average

velocity magnitudes were at the middle depth at 1.9 ft/s, with slightly higher average velocity magnitudes at the surface at 2.0 ft/s, and the highest average velocity magnitudes at the bottom depth at 2.2 ft/s. The ADV used could not measure the vertical component of the velocity vector and thus the velocity and TKE measurements presented represent minimum values. However, observations from the string apparatus revealed that the measurement locations were not dominated by the vertical velocity component (Figure 26) and thus the values of the vertical components may be low.

The spatial distribution of TKE values was opposite to velocity vectors in the longitudinal direction but similar with depth. The highest TKE values throughout each pool were focused in pockets on the upstream end of the pools in the centerline as shown in Figure 12. Near the top of the fishway in the centerline of the third pool from the top, TKE values were approximately 0.31 m^2/s^2, and increased moving downstream along the fishway. In the second pool from the bottom of the fishway TKE values were approximately 1.3 m^2/s^2. However, at depth the TKE values along the centerline decreased with average TKE values in the centerline at the surface, middle, and bottom depths of approximately 0.37 m^2/s^2. 0.25 m^2/s^2, and 0.12 m^2/s^2, respectively. The maximum TKE values were located in the pockets on the upstream end of the pools along the centerline and the maximum values at the surface, middle, and bottom depths were approximately 1.26 m^2/s^2, 0.42 m^2/s^2, and 0.18 m^2/s^2, respectively. These maximum TKE values are similar to those in Guiny et al. (2005) who calculated a maximum TKE range for a pool and weir fishway with one orifice per weir at 0.4 m^2/s^2 to 1.2 m^2/s^2 and suggest that these values may represent a range of maximum TKE values that would provide

favorable fish passage conditions depending on species. The spatial distribution of TKE values in the new design concentrates the highest TKE values to a small area leaving large portions of the fishway available with low TKE values which are generally thought to be preferred by Pacific salmonids. At the sides of the pools TKE values, similarly to the velocity vectors, were low with an average TKE value of approximately 0.08 m^2/s^2 at all depths.

The width of the streaming flow in the centerline was measured using a point gauge and visual observation and represents a prototype width of 8 feet. Velocities in the centerline and at the surface, and especially in the upstream portion of the centerline were measured to reach a maximum of 9.10 ft/s and average 6.81 ft/s which may require fish to swim at or near burst swim mode. From Table 3 the average velocity in the centerline of 6.81 ft/s is much larger than the average velocity at the pool sides and surface depth of 2.03 ft/s. The highest TKE values were shown to be concentrated in the same area as the highest velocities in the upstream portion of the centerline at the surface with an average TKE value along the centerline at the surface of 0.37 m^2/s^2. These higher velocities in the centerline and surface depth would require fish to expend more effort swimming and additional energy expenditure to stabilize their position due to high TKE values. At the middle and bottom depth in the centerline, velocities and TKE values are much lower than at the surface and are relatively similar to the velocity magnitudes at the pool sides. However, the velocity vectors along the centerline at the bottom depth are in the upstream direction, which may not be preferred by anadromous fish as they are known to

orient and swim against the flow. Thus, fish passage along the centerline at this flow rate would not be a preferred pathway.

A quick calculation of some of the passage conditions in the centerline of the fishway reveal that it is the most energy expensive for fish. Considering the mean, median and mode fish fork length of both steelhead and coho salmon it would be fair to assume a fork length of 2 feet for calculations. If a fish were to attempt to migrate through the centerline of the fishway it would encounter a velocity of approximately 9 ft/s for approximately 6 feet of travel distance. With a 2-foot fish and a 9 ft/s water velocity, the water velocity can be expressed as 4.5 BL/s. Assuming a minimum ground prolonged swim speed of 1.5 BL/s, the total swim speed of this fish is approximately 6 BL/s. Data from Figure 22 suggest that when a prolonged swim speed of 6 BL/s is held constant a fish would reach 100 F% in approximately 20 seconds. At 6 BL/s for 6 feet of travel distance it would take approximately one second. Although this amount of time does not fatigue fish excessively, it is a significant portion of time and energy for a relatively short amount of distance traveled. This basic calculation supports the claim that the centerline would be the least efficient pathway for fish passage.

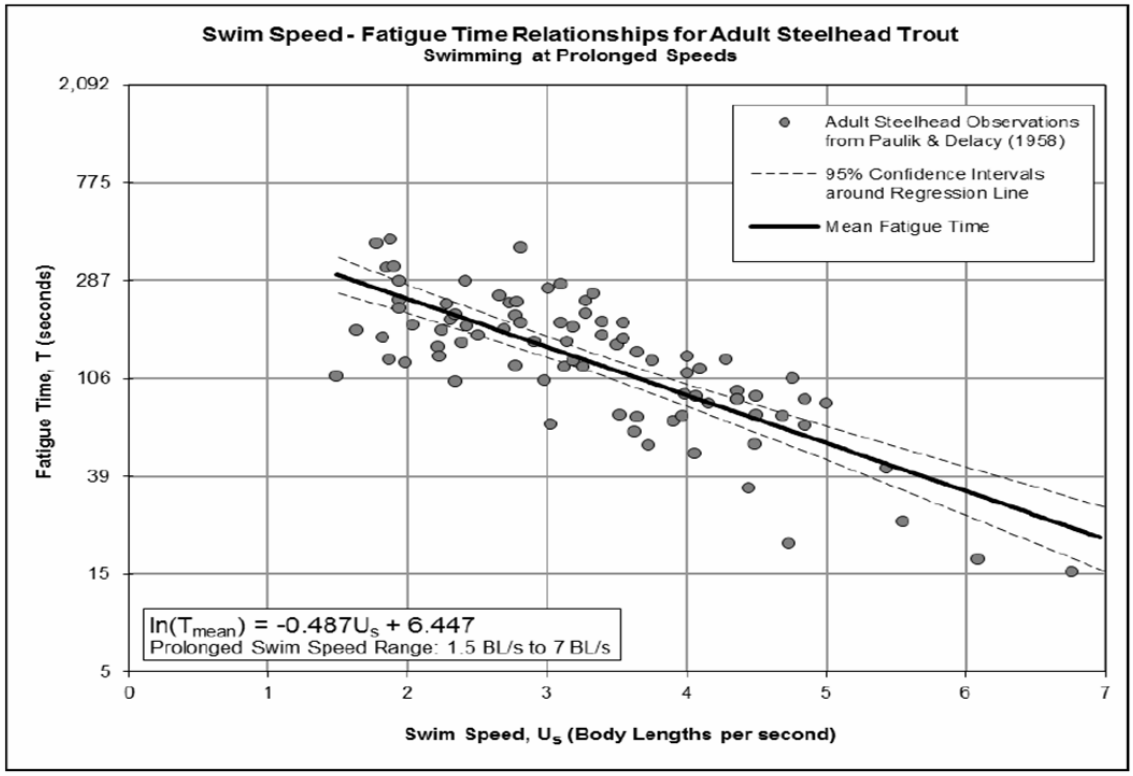

Figure 22. Relationship of swim speed versus fatigue time for steelhead swimming at prolonged swim speeds, developed by (Love & James, 2016), using data presented in (Paulik & DeLacy, 1957).

Another passage model scenario was analyzed in addition to the scenarios considered in this thesis where coho salmon, the weaker swimmers, were sent through the centerline of the fishway in a straight path along which velocities and TKE values are highest. One thousand coho salmon were simulated to ascend the prototype fishway in this scenario and 100 replicates of 1000 coho salmon were completed. Under this scenario the percentage of fish that reached 100 F% or higher ranged from 34.5% to 39.9%. Although reaching 100 F% does not imply overall passage failure, it does suggest that the centerline is not an energetically optimal path. It is theorized from an

evolutionary perspective that fish may chose a distance optimizing path in their migration (Castro-Santos, 2005), which may likely include pathways with low velocities and turbulence which in this fishway occur at the sides of the pools. Fish that swim in the centerline will likely incur enough fatigue that they will need to rest before continuing to migrate. This means that all three swim modes could potentially be used with burst mode used to negotiate the weirs, prolonged mode used to swim in pools, and sustained mode used to rest.

At the sides of the pools, lower velocities and TKE values provide more favorable passage conditions compared to the centerline. The velocity vectors follow defined eddy circulations that provide continuous pathways that do not fluctuate much for fish to migrate efficiently. The results of the passage model along the straight and long pathway presented in the results section suggest that the sides of the pools at all depths throughout the fishway will be the most efficient place for passage. In the design prototype fishway the mean F% for 100 replicates of 1000 fish for the passage scenarios at the high flow rate, for steelhead and coho salmon range from 42.0-53.5 F%, and not a single fish reached 100 F%.

The skewness and kurtosis results were similar across all flow rates and indicate that both the longitudinal and lateral eddies within each pool throughout the fishway experience few intermittent turbulent fluctuations. The results also indicate that the few turbulent fluctuations were asymmetrical which means they will not fluctuate in the same direction every time. These results mean that the various flow pathways throughout the

fishway are mostly continuous and predictable which may be advantageous for fish to exploit when choosing the most energetically optimum migration pathway.

Medium Flow

The average velocities and TKE values at the medium flow rate are reduced in almost all location in the fishway compared to the high flow rate. The only locations where average velocities increased were at the middle and bottom depth of the centerline, whose average velocities increased by 0.68 ft/s and 0.17 ft/s, respectively. Since the centerline changed from streaming to transitional flow there is a small longitudinal eddy rotating in clockwise direction when looking at a side view shown in Figure 1. There is no streaming flow in the centerline but a transitional flow instead. The flow direction of the lateral eddies in the pool sides at the medium flow rate are the same as for the high flow rate. There is transitional flow in the centerline and the sides of the pools and plunging flow near the side walls. The vectors of plunging flow do not match those described for a pool-and-weir fishway because the weir geometry is such that it creates multiple eddies and forces flow into certain directions. Overall, the passage conditions appear to be more accommodating at the medium flow rate, as there is no streaming flow and velocities and TKE values are reduced in general. In the design prototype fishway the mean F% for 100 replicates of 1000 fish for the passage scenarios at the medium flow rate, for steelhead and coho salmon range from 41.2-52.9 F%, and not a single fish reached 100 F%.

Low Flow

The average velocities and TKE values at the low flow rate are lower throughout most of the fishway compared to the medium flow rate. The only locations where velocities increased on average were at the middle and bottom depth of the centerline, whose average velocities increased by 0.32 ft/s and 1.4 ft/s, respectively. Otherwise the low flow seems to have the same flow regime, combined transitional and plunging, as the medium flow rate. Of the three flow rates tested, the low flow rate appears to possess the largest region where passage can be efficient for steelhead and coho salmon. The low flow rate was not evaluated using the passage model because efficient passage was already calculated for the larger two flow rates which would be more difficult for fish to pass.

Percent Fatigue and Ascension Times

F% was shown to be more sensitive to pathway than flow rate. One possible reason for this result is that differences in the velocity magnitudes between flow rates along the predetermined pathways on the pool sides were similar, whereas the difference in travel distance between the straight and long pathways were significant.

Passage through the proposed fishway was found to be more difficult for coho salmon than steelhead but adults of both species were predicted to pass successfully. F% was estimated to be between 3.5-5.5 F% higher on average for coho salmon than steelhead. This is a result of coho salmon being slightly weaker swimmers than steelhead,

which is captured in the equation parameters derived from measurements of swim performance (Figure 22). Another cause of the disparity in performance is the coho salmon fork length data used for the Monte Carlo simulations show that the mode coho salmon fork length was 2 inches smaller than the mode steelhead fork length. Using smaller fork lengths in the model equations will also produce higher F%.

For the design length fishway, no scenario resulted in fish reaching 100 F%. This result indicates that the prototype fishway, will not delay passage through the fishway due to fatigue. However, it is also important to note the differences in performance between coho salmon and steelhead. Steelhead incurred less mean F% than coho salmon for every scenario, but the standard deviations of the eight designed length scenarios ranged from 1.9-4.5 F% for both steelhead and coho salmon which could potentially bridge the performance gap between them.

It cannot yet be determined if the ascension times calculated from the passage model accurately represent reality. The maximum ascension time calculated for all scenarios for the prototype fishway at design length was 119.1 seconds. Generally, the ascension times produced by the passage model may be considered quick because of some of the model's simplifying assumptions, especially continuous swimming, and since none of the fish reached 100 F% there were no periods of rest that would have increased ascension times. Although predicted ascension times may be too fast, comparisons between relative ascension times are instructive. Differences in ascension times between the medium and high flow rate for the design fishway length ranged from 1.3-6.2 seconds, or about 1-6% for both steelhead and coho salmon. These differences are

relatively low and suggest that ascension time was not sensitive to differences in flow rate. However, the ascension times were slightly higher under the medium flow rate compared to the high which contradicts Keefer et al. (2004) who found quicker ascension times at lower flow rates. The slightly higher ascension times calculated for the medium flow rate are accounted for by the equations used in the passage model that increase the swim speed when velocities are increased. Like F%, ascension times may not have been sensitive to flow rate because the difference between the velocity magnitudes along these pathways at the two flow rates evaluated were not significantly different. However, pathway did have an effect on ascension times. Differences in ascension times between the straight and long pathways for the design fishway length ranged from 24.3-35.1 seconds for both steelhead and coho salmon. These results show that the long path adds between 24.3-35.1 seconds depending on the scenario, which represents a significant portion of the overall ascension times calculated. The model considered two predetermined pathways and flow rates, for two species that have relatively similar swimming abilities, where the water velocities along they the two pathways were also similar because they were both in zones designed to have low velocities regardless of flow rate within the fish passage design flow range. The differences in passage efficiency in all scenarios considered were thus explained by the differences in the two pathways.

Fishway Extension

The passage model determined that the prototype fishway could be extended up to three sets of pools and weirs, equal to a 37.5 feet increase in length without a fish of either species reaching 100 F% under any scenario. However, it is reasonable to expect there may be delays from inherent preferred behaviors including motivational delays. Not extending the fishway length to the point of achieving 100 percent fatigue provides an energetic factor of safety for variances in performance and behavioral delays.

CONCLUSION

Insights into the hydraulics of this new pool-and-chute, vortex weir fishway design have been gained by direct measurement in a 1:15 scale physical model. These data include information about velocity vectors, TKE, and other turbulence statistics. Additionally, a preliminary passage model was developed to estimate the amount of fatigue that would be incurred by steelhead and coho salmon ascending this prototype fishway and the amount of time needed for successful passage. Prior to this investigation, information regarding the hydraulics of pool-and-chute fishways remained limited and information regarding this unique design could only be found from a single source, Nyberg et al. (2016). The following research questions posed in the beginning of this thesis have been answered to varying extents including:

1. The velocity vectors have been directly measured in the physical scale model which revealed the velocity magnitudes and directions. These values were scaled up for estimations of the prototype values over each of the three flow rates.
2. The TKE values have been calculated for the physical scale model and reveal the magnitude and spatial distribution of turbulence. These values were scaled up for estimations of the prototype TKE values for each of the three flow rates.
3. Continuous migration pathways exist throughout the fishway at the three fish passage design flows considered. At the high flow rate, the best passage pathways utilize the pool sides outside of the streaming flow regime. Streaming flow conditions were only observed at the high flow rate and this region would not

provide an energy efficient passage corridor because it would require continuous use of burst swim mode. At the medium and low flow rates, continuous passage pathways exist throughout the fishway, where fish can use lower speed swim modes to swim in the pools and reserve burst swim mode for negotiating the weirs.

4. Mean and median F% for steelhead and coho salmon for the designed fishway length for 100 replicates of 1000 fish for each passage scenario are both below 53.5 F% and no simulated scenarios resulted in a single fish reaching 100 F%.
5. The passage model determined that the prototype fishway could be extended up to three sets of pools and weirs, equal to a 37.5 feet increase in length without a fish reaching 100 F% under any scenario.

In general, the passage model suggests a high passage efficiency over the flow rates considered. However, it is unlikely that the prototype design will actually produce 100% passage efficiency as the model suggests with no fish reaching 100 F%. Some potential reasons for the likely differences between the model and reality include factors not considered in this thesis and thus warrant further investigation. Behavioral and motivational delays leading to increased fatigue were not considered and are still poorly understood. The passage model assumes fish begin ascension of the fishway with zero percent fatigue however, when fish reach these structures in coastal rivers and tributaries it is unlikely that they have zero percent fatigue. Another factor that warrants further investigation is how fish will respond to the fishway and its entrance efficiency. Also,

calibrating the passage model with observed swim speeds from a full-scale prototype installation and quantifying possible error from scale effects in the hydraulic measurements would improve the passage model. Insights into these factors would provide a more complete perspective of the efficacy of this fishway design in the broader context of fish passage.

REFERENCES

Alaska Steeppass Fishways by Sheepscot Machine Works. 2017. Alaska Steeppass Fishways. Newcastle, ME.

Allen, S., Love, M. & Llanos, A.. 2004. Peacock Creek Pool and Weir Fishway. Technical Report for California Department of Fish and Wildlife: Grant # P0110300.

Baki, A., Zhu, D. & Rajaratnam, N.. 2014. Turbulence Characteristics in a Rock-Ramo-Type Fish Pass. Journal of Hydraulic Engineering, pp. 1-14.

Bates, K.. 1991. Pool-and-Chute Fishways. American Fisheries Society Symposium, pp. 268-277.

Bates, K.. 2001. Fishway Design Guidelines for Pacific Salmon, Working paper 1.6 9/2001: Washington Department of Fish and Wildlife.

Brett, J.. 1964. The Respiratory Metabolism and Swimming Performance of Young Sockeye Salmon. Journal of the Fisheries Research Board of Canada, pp. 21(5): 1183-1226.

Bunt, C. M., Castro-Santos, T. & Haro, A.. 2012. Performance of Fish Passage Structures at Upstream Barriers to Migration. River Research and Applications, Issue 28, pp. 457-479.

Calluaud, D., Cornu, V., Bourtal, B., Dupuis, L., Refin, C., Courret, D., David, L.. 2012. Scale effects of turbulence flows in vertical slow fishways: field and laboratory measurement investigation. 9th International Symposium on Ecohydraulics, pp. 1-9.

Castro-Santos, T.. 2005. Optimal swim speeds for traversing velocity barriers: an analysis of volitional high-speed swimming behavior of migratory fishes. Journal of Experimental Biology, pp. 208:421-432.

Castro-Santos, T.. 2006. Modeling the effect of varying swim speeds on fish passage through velocity barriers. Trans. American Fisheries Society, pp. Vol 135, Issue 5, pp 1230-1237.

CDFG, California Department of Fish and Game. 1998. California Salmonid Stream Habitat Restoration Manual Part III, Sacramento, CA.

CDFG, California Department of Fish and Game. 2002. Culvert Criteria for Fish Passage, Sacramento, CA.

CDFW, California Department of Fish and Wildlife. 2009. Fish Passage Design and Implementation, Sacramento, CA.

Chanson, H.. 2008. Acoustic Doppler Velocimetry (ADV) in the Field and in Laboratory: Practical Experiences. Department of Civil Engineering Brisbane, Australia: University of Queensland.

Clay, C.. 1995. Design of Fishways and Other Fish Facilities Second edition. United States of America: Lewis Publishers.

Davidson, P.. 2015. Turbulence: An introduction for scientists and engineers, second edition. United Kingdom: Oxford University Press.

Ead, S. A., Katopodis, C., Sikora, G. J. & Rajaratnam, N.. 2004. Flow Regimes and Structure in Pool and Weir Fishways. Journal of Environmental Engineering and Science, Issue 3, pp. 379-390.

Guiny, E., Ervine, D. & Armstrong, J.. 2005. Hydraulic and Biological Aspects of Fish Passes for Atlantic Salmon. Journal of Hydraulic Engineering, 131(7).

Haro, A., Castro-Santos, T., Noreika, J. & Odeh, M.. 2004. Swimming performance of upstream migrant fishes in open-channel flow: a new approach to predicting passage through velocity barriers. Canadian Journal of Aquatic and Fisheries Sciences, Issue 61, pp. 1590-1601.

Hinch, S. & Rand, P.. 2000. Optimal swimming speeds and forward-assisted propulsion: energy-conserving behaviours of upriver-migrating adult salmon. Canadian Journal of Fish and Aquatic Science, pp. 57, 2470-2478.

Hockley, F., Wilson, C., Brew, A. & Cable, J., 2013. Fish responses to flow velocity and turbulence in relation to size, sex and parasite load. Journal of the Royal Society, p. 11.

Houghtalen, R., Akan, A. & Hwang, N.. 2010. Fundamentals of Hydraulic Engineering Systems Fourth Edition. Boston: Pearson Higher Education Inc.

Hunter, L. & Mayor, L.. 1986. Analysis of fish swimming performance data. p. 96 pages.

Keefer, M.L., Peery, C.A., Bjornn, T.C., Jepson, M.A., Stuehrenberg, L.C.. 2004. Hydrosystem Dam, and Reservoir Passage Rates of Adult Chinook Salmon and

Steelhead in the Columbia and Snake Rivers. Transactions of the American Fisheries Society, 133:1413-1439.

Kiernan, J. et al., 2016. Results of Scott Creek Life Cycle Monitoring Station 2014-2016. Final Report Submitted to the California Department of Fish and Wildlife as part of the Requirements of FRGP Award # P1330409.

Kirkbride, A.. 1993. Observations of the influence of bed roughness on turbulence structure in depth limited flows over gravel beds. pp. Turbulence: perspectives on flow and sediment transport. Chichester, UK: Wiley.

Kleinschmidt. 2017. Denil fishway - South Berwick Fish Passage Project. South Berwick, ME.

Lacey, J., Neary, V.S., Liao, J.C., Enders, E.C., Tritico, H.M.. 2012. The IPOS Framework: Linking Fish Swimming Performance in Altered Flows from Laboratory Experiments to Rivers. River Research and Applications, pp. 28: 429-443.

Lang, M., Love, M. & Trush, W.. 2004. Improving Stream Crossings for Fish Passage, Rep. No. 50ABNF800082: National Marine Fisheries Service.

Liao, J.. 2007. A review of fish swimming mechanics and behaviour in altered flows. The royal society, Volume 362, pp. 1973-1993.

Liao, J., Beal, D., Lauder, G. & Triantafyllou, M.. 2003. The Kármán gait: novel kinematics of rainbow trout swimming in a vortex street. Journal of Experimental Biology, pp. 206,1059-1073.

Love, M.. 2006. Letter Report: Assessment of Fish Passage Conditions at the Niles Canyon Flow Measurement Weir on Alameda Creek, California. Prepared for the Federation of Fly Fishers.

Love, M.. 2015. Fishway Design Briefing Interview, 2015.

Love, M. & James, T.. 2016. Technical Memorandum: Branciforte Creek Flood Control Channel Fish Passage Assessment, Santa Cruz, CA.

Love, M. & Llanos, A.. 2006. Preliminary fish ladder concept design for Corte Madera Creek flood control channel, for transition between units three and four., Arcata: Michael Love & Associates.

Michael Love and Associates. 2012. Pool-and-chute fishway on San Anselmo Creek, CA. Marin county, CA.

Michigan Department of Natural Resources. 2017. Berrien Springs Fish Ladder. Grand Rapids, MI.

Montgomery, J., McDonald F., Baker, C.F., Carton, A.G., Ling, N.. 2003. Sensory integration in the hydrodynamic world of rainbow trout. Proc. Royal Society B, pp. 270, S195-S197.

Nau, R.. 2016. Stationarity and differencing, Durham, North Carolina.

NMFS, National Marine Fisheries Service. 2008. Anadromous Salmonid Passage Facility Design. Portland, OR(Oregon): National Marine Fisheries Service, Northwest Region.

NOAA, National Oceanic and Atmospheric Administration. 2001. Guidelines for salmonid passage at stream crossings, 14 pages: NOAA SW Region.

Noonan, M., Grant, J. & Jackson, C. D.. 2012. A quantitative assessment of fish passage efficiency. Fish and Fisheries, Volume 13, pp. 450-464.

Nyberg, M. Draeger, B., Weeekly, B.. Cashman, E.. 2016. Analysis of Vortex Pool-and-Chute Fishway. American Journal of Undergraduate Research, 13(4), pp. 37-57.

Paulik, G. & DeLacy, C.. 1957. Swimming abilities of upstream migrant silver salmon, sockeye salmon and steelhead at several water velocities. Seattle (Washington): University of Washington, School of Fisheries.

Shapovalov, L. & Taft, A.. 1954. The life histories of the steelhead rainbow trout (Salmo gairdneri gairdneri) and silver salmon (Oncorhynchus kisutch) with special reference to Waddell Creek, California, and recommendations regarding their management. Calif. Dept. Fish and Game, Fish Bull. No. 98, 375 pp.

Smith, D.. 2003. The shear flow environment of juvenile salmonids. PhD thesis, University of Idaho.

SonTek. 1997. Pulse Coherent Doppler Processing and the ADV Correlation Coefficient. San Diego, CA.

SonTek. 2001. SonTek/YSI ADVField/Hydra Acoustic Doppler Velocimeter (field) Technical Documentation, San Diego, CA.

Towler, B., Mulligan, K. & Haro, A.. 2015. Derivation and application of the energy dissipation factor in the design of fishways. Journal of Ecological Engineering, Volume 83, pp. 208-217.

Tritico, H.. 2009. The effects of turbulence on habitat selection and swimming kinematics of fishes. PhD dissertation, Civil and Environmental Engineering, University of Michigan, p. 155.

Voulgaris, G. & Trowbridge, J.. 1998. Evaluation of the Acoustic Doppler Velocimeter (ADV) for Turbulence Measurements. Journal of Atmospheric and Oceanic Technology, Volume 15, pp. 272-289.

Wahl, T.. 2004. WinADV Manual, Denver: U.S. Bureau of Reclamation.

Warhaft, Z.. 2002. Turbulence in nature and in the laboratory. Proc. National Academy of Sciences, pp. USA 99, 2481-2486.

Weaver, C.. 1963. Influence of water velocity upon orientation and performance of adult migrating salmonids. U.S. Fish and Wildlife Service.

Webb, P.. 1998. Entrainment by river chub Nocomis micropogon and smallmouth bass Micropterus dolomieu on cylinders. Journal of Experimental Biology, pp. 201, 2403-2412.

Webb, P. & Cotel, A.. 2010. Turbulence: does vorticity affect the structure and shape of body and fin propulsors?. Integrative and Comparative Biology, 6(50), pp. 1155-1166.

White, F., 2011. Fluid Mechanics. New York(NY): McGraw Hill.

APPENDICES

Thirty-seven flow measurements and stage heights collected from the flume head tank and flow over the V-notch weir are plotted in Figure 23, in the appendix. These measurements were taken by me and numerous Humboldt State University students over the past ten years. The V-notch weir rating curve shows a strong relationship between the flow rate measured and the stage height in the head-tank ($r^2 = 0.9951$). The residuals shown in Figure 24 revealed that there is no bias in the data. The three head tank elevations used in this thesis were 9.81, 10.25, and 10.75 inches. The residuals do not exceed +/- 0.015 cfs for any head tank elevation measured in the calibration. When analyzing the average residuals and flow rates at the three flow rates used in this thesis the percent error does not exceed 10%.

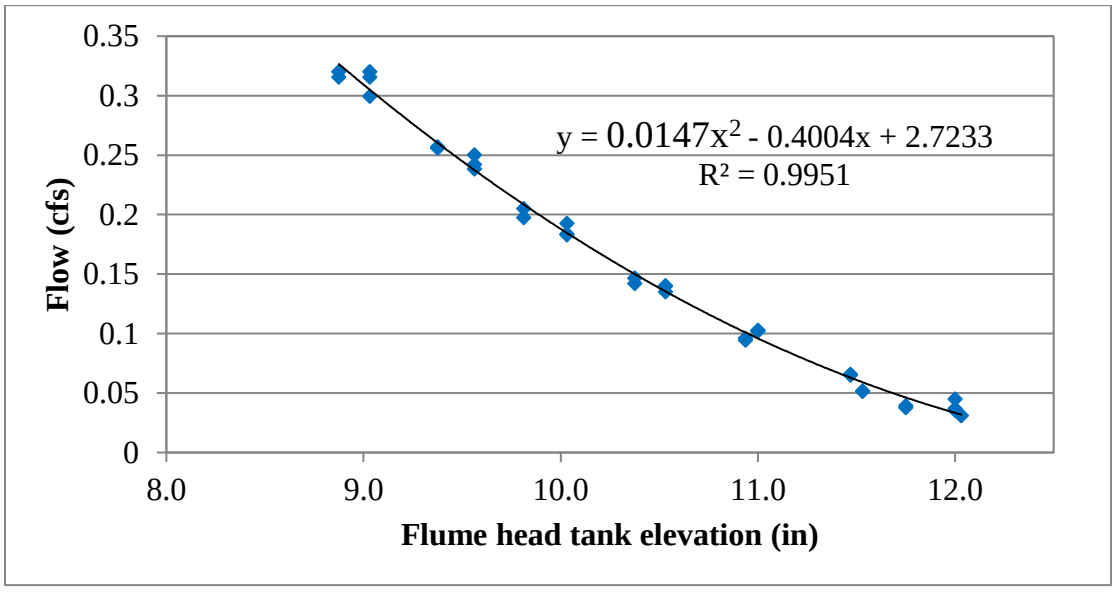

Figure 23. Rating curve for the flume flow rate, head tank elevation.

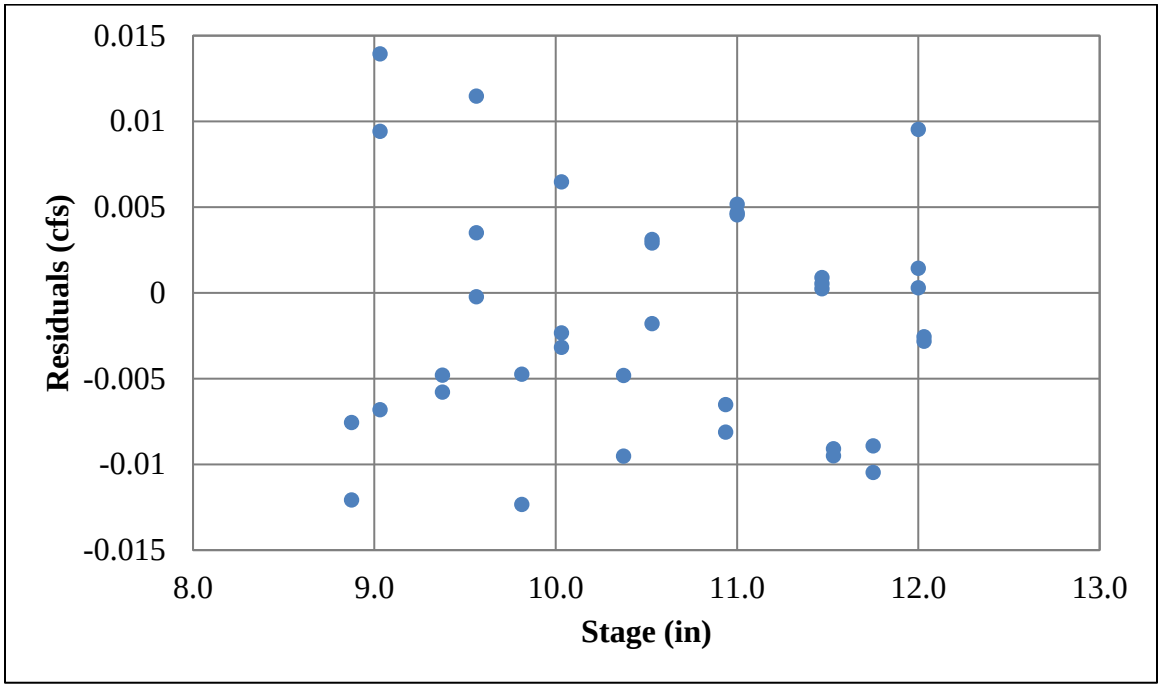

Figure 24. Residuals in cfs for the flume v-notch weir calibration.

The three flow rates used for this thesis were directly measured in the flume by capturing and weighing flow over the V-notch weir during a timed interval. Additional flow rates were also measured and a rating curve was produced to allow quick determinations of other flows for further investigations. A regression of rating curve data shows a strong relationship and the function of the trend line estimates flow rates very close to the measured flow rate. The amount that the rating curve underestimated or overestimated was relatively small with no distinct stage heights that would consistently either underestimate or overestimate the flow rate.

Table 14. Raw data, percent difference, and relative percent difference of the two set of velocity measurements taken for pool F.

Position	Avg Vx Rerun (cm/s)	Avg Vy Rerun (cm/s)	Avg Vx Orig (cm/s)	Avg Vy Orig (cm/s)	% Difference	Relative % Difference
F01-B	2.8434	-1.4729	2.5438	-4.6552	40	49
F01-M	6.8403	1.8956	6.7641	-1.8144	1	1
F01-S	13.5434	1.5007	14.2467	-5.38	11	11
F02-B	17.228	3.257	13.0477	4.9474	26	23
F02-M	13.3661	0.0121	13.5034	-0.0181	1	1
F02-S	13.4345	-1.4006	12.8803	1.0851	4	4
F03-B	25.9574	3.9445	25.4234	3.4687	2	2
F03-M	9.9707	7.7787	11.6657	7.7132	10	10
F03-S	2.8211	8.9541	-0.2612	9.83	5	5
F04-B	6.9693	5.7266	3.7289	4.5388	54	42
F04-M	26.4955	17.1341	27.5031	17.1405	3	3
F04-S	32.9306	19.0557	35.2274	18.2561	4	4
F05-B	14.2483	19.0053	12.7028	18.4917	6	6
F05-M	11.1391	8.4943	11.731	6.8896	3	3
F05-S	11.7	-2.7739	11.4934	-3.8575	1	1
F06-B	8.5533	12.9199	11.3853	9.8278	3	3
F06-M	4.4128	10.9548	4.4518	5.7172	63	48
F06-S	3.7377	12.8449	4.2369	12.29	3	3
F07-B	-13.2389	-4.5165	-12.9614	-8.4766	10	10
F07-M	-10.4255	-0.4607	-9.3011	-3.1687	6	6
F07-S	-17.9914	2.9669	-18.0358	1.8946	1	1
F08-B	-10.0735	-12.0167	-7.9841	-11.2298	14	13
F08-M	-10.2558	-8.438	-10.0557	-8.6772	0	0
F08-S	-13.1206	-5.9363	-14.0058	-7.7976	10	11
F09-B	18.3444	-0.985	25.9242	3.6634	30	35
F09-M	12.8478	-3.1703	14.9829	-3.7724	14	15
F09-S	11.3916	-6.5735	9.8427	-10.1631	7	7
F10-B	0.3363	-0.2182	1.0004	-0.1868	61	87
F10-M	25.1918	12.5865	24.1797	12.308	4	4

Position	Avg Vx Rerun (cm/s)	Avg Vy Rerun (cm/s)	Avg Vx Orig (cm/s)	Avg Vy Orig (cm/s)	% Difference	Relative % Difference
F10-S	6.6582	-8.3722	5.5167	-8.7527	3	3
F11-B	8.3399	4.7904	7.1618	3.7783	19	17
F11-M	-2.9012	-1.5804	0.2191	0.7977	299	120
F11-S	-44.5842	-31.0851	-38.1609	-29.8152	12	12
F12-B	18.8688	1.5227	19.5358	2.4007	4	4
F12-M	-15.2718	-3.3684	-12.0098	-1.2494	30	26
F12-S	5.375	-11.6113	9.091	-8.1995	5	4
F13-B	-0.3489	-11.5221	3.066	-11.2422	1	1
F13-M	5.8604	-12.2901	6.8803	-11.7281	0	0
F13-S	6.2544	-12.5746	6.4303	-12.0535	3	3
F14-B	15.4158	-2.3968	16.1962	-3.224	6	6
F14-M	16.2191	-3.226	14.5094	-4.6653	9	8
F14-S	14.3785	-2.591	13.4532	-5.0196	2	2

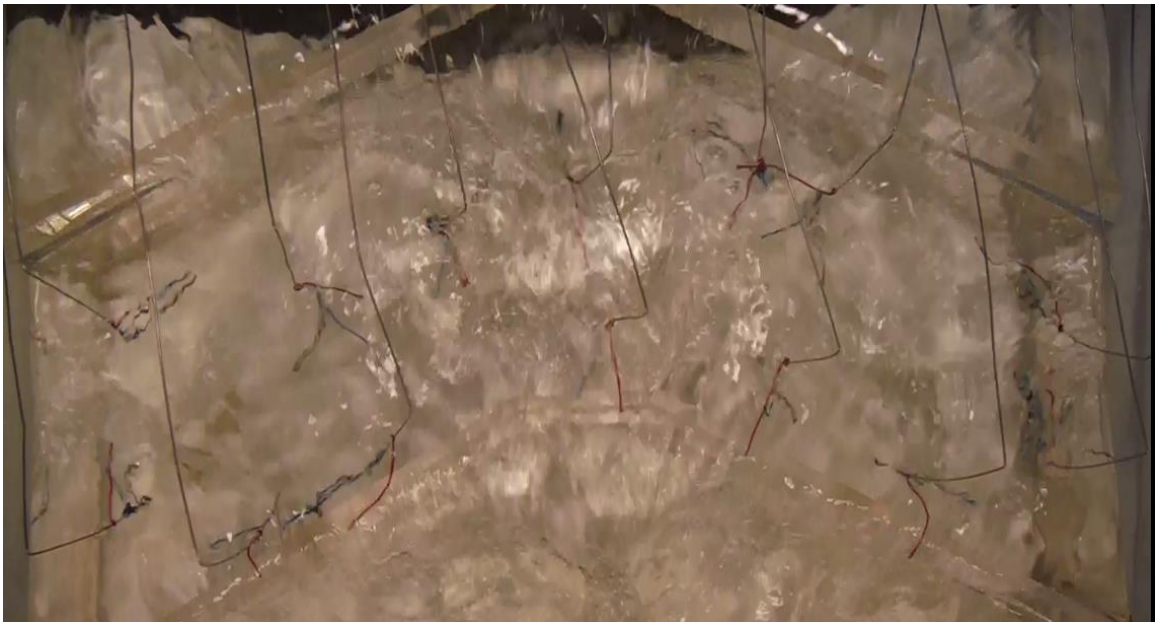

Figure 25. Plan View image of the string apparatus at the medium flow rate.

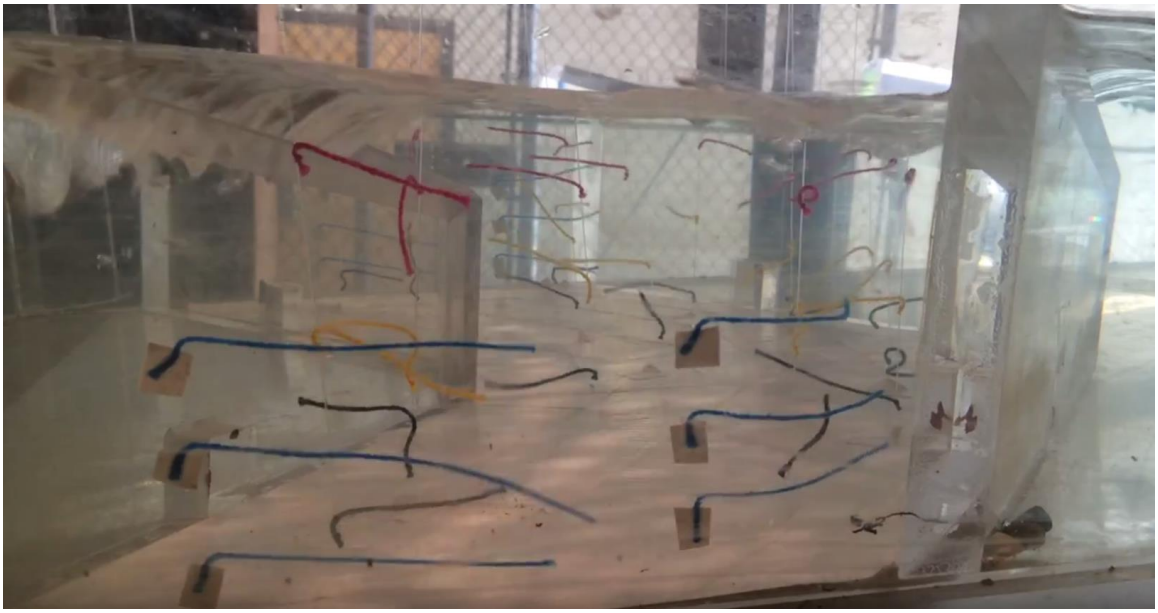

Figure 26. Side view image of the string apparatus at the medium flow rate.

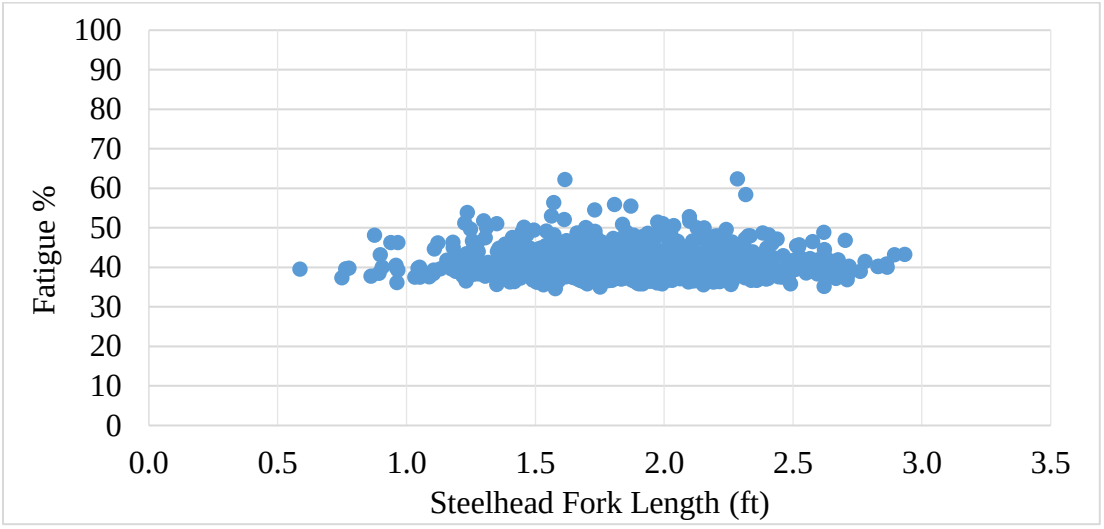

Figure 27. Plot of one thousand simulated Steelhead and their percent fatigue from completing the ascension of the prototype fishway on the straight pathway for the medium flow rate.

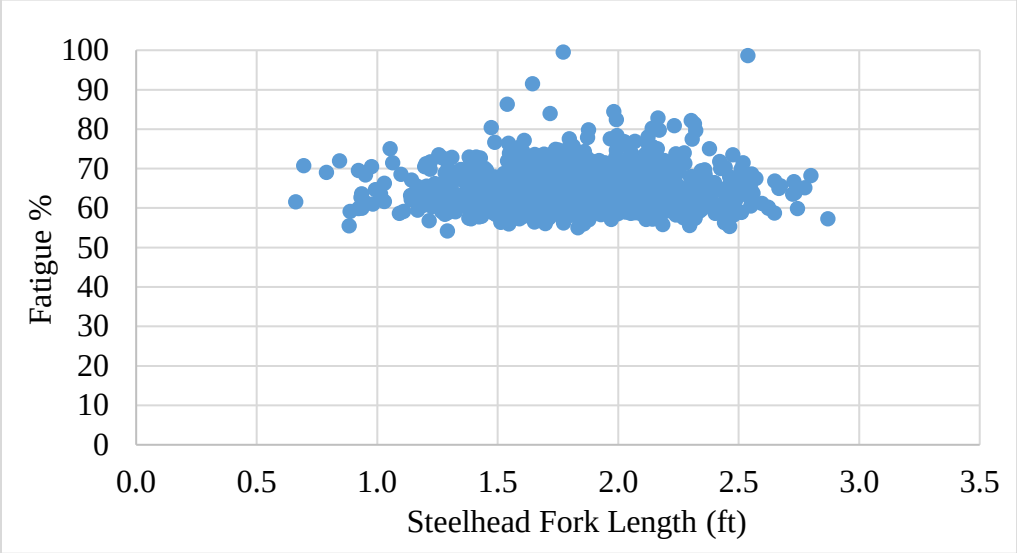

Figure 28. Plot of one thousand simulated Steelhead and their percent fatigue from completing the ascension of an extended prototype fishway on the straight pathway for the medium flow rate.

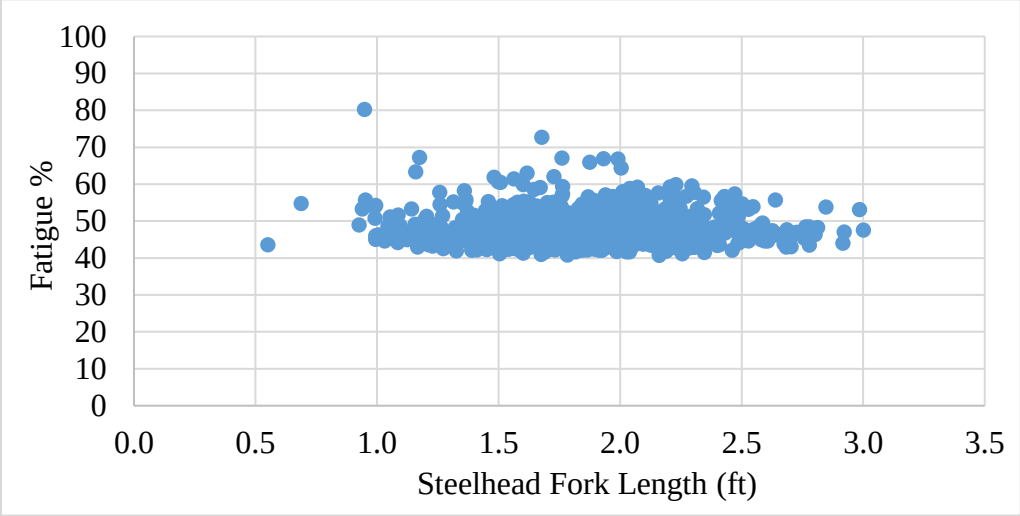

Figure 29. Plot of one thousand simulated Steelhead and their percent fatigue from completing the ascension of the prototype fishway on the long pathway for the medium flow rate.

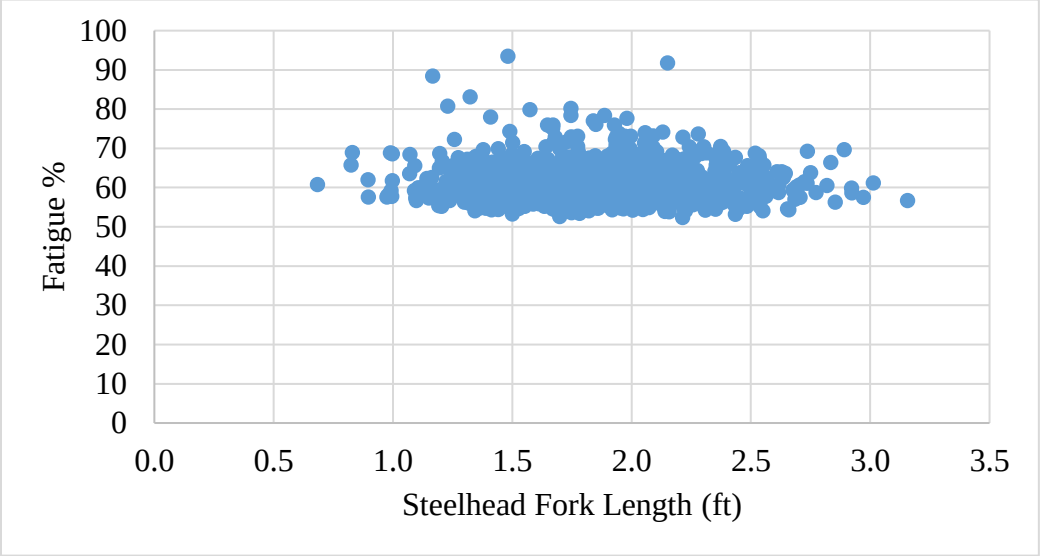

Figure 30. Plot of one thousand simulated Steelhead and their percent fatigue from completing the ascension of an extended prototype fishway on the long pathway for the medium flow rate.

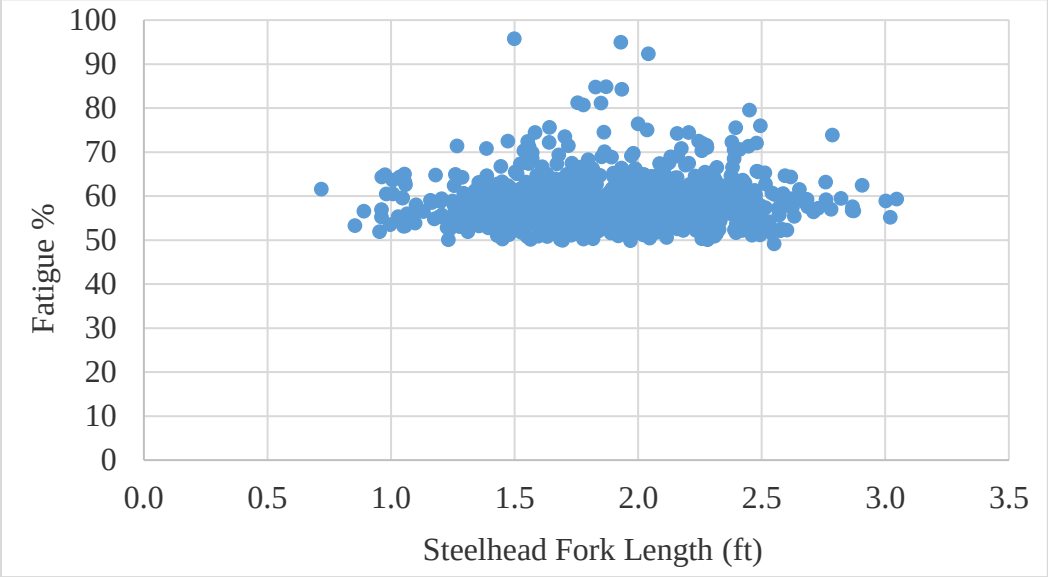

Figure 31. Plot of one thousand simulated Steelhead and their percent fatigue from completing the ascension of an extended prototype fishway on the straight pathway for the high flow rate.

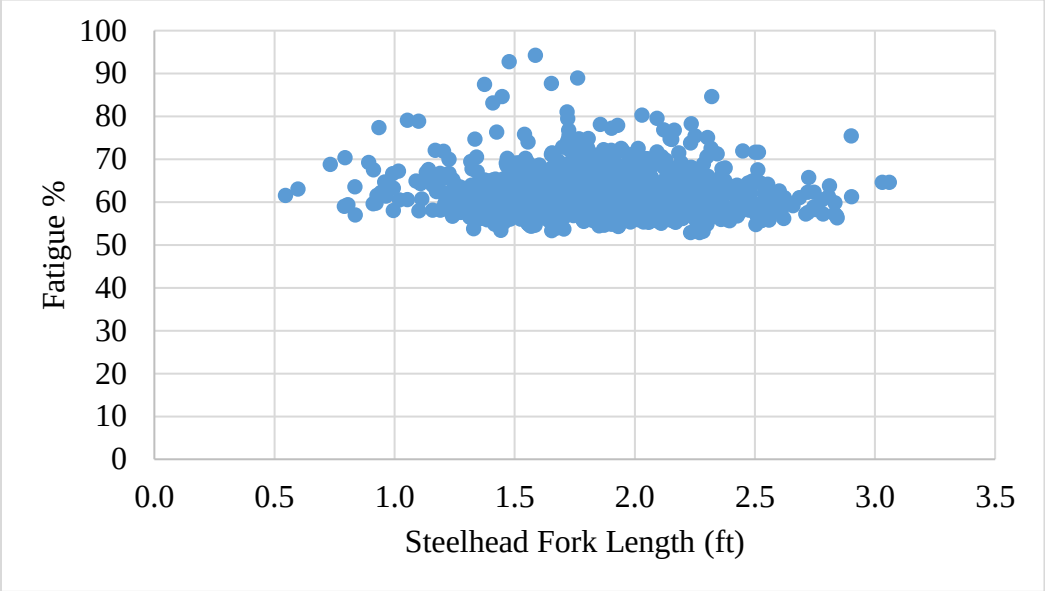

Figure 32. Plot of one thousand simulated Steelhead and their percent fatigue from completing the ascension of an extended prototype fishway on the long pathway for the high flow rate.

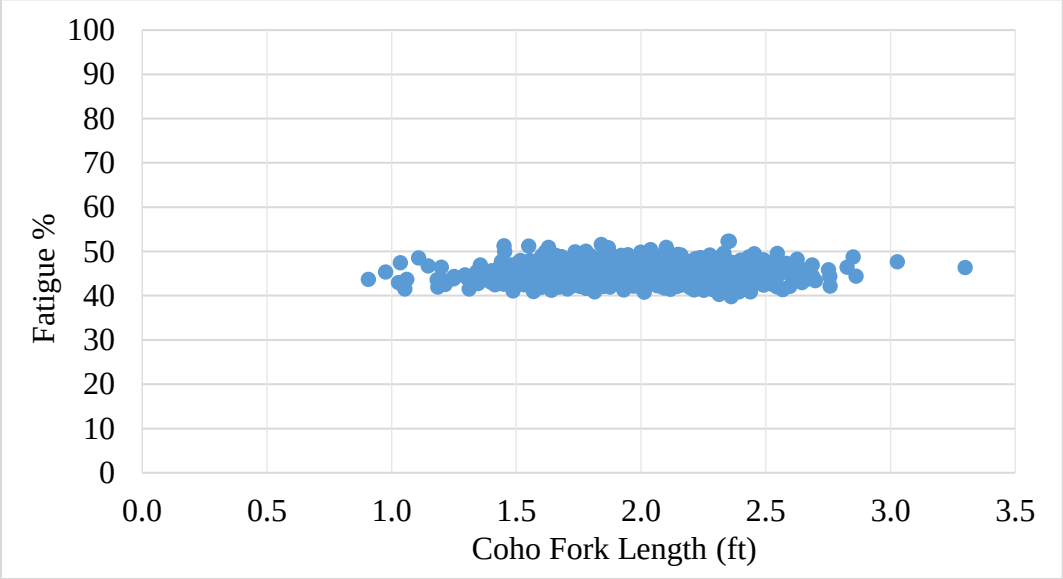

Figure 33. Plot of one thousand simulated Coho salmon and their percent fatigue from completing the ascension of the prototype fishway on the straight pathway for the medium flow rate.

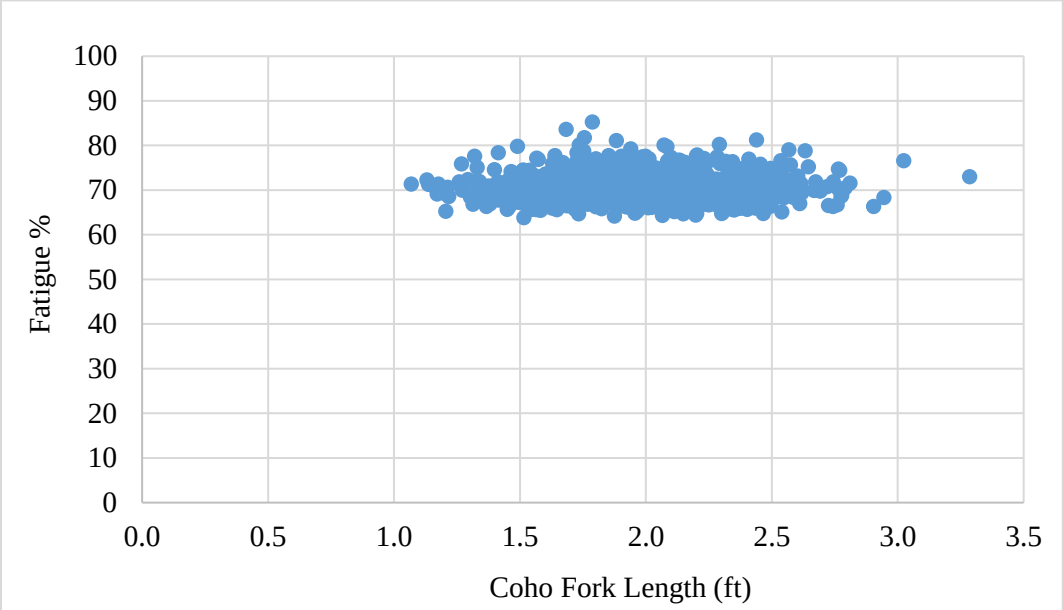

Figure 34. Plot of one thousand simulated Coho salmon and their percent fatigue from completing the ascension of an extended prototype fishway on the straight pathway for the medium flow rate.

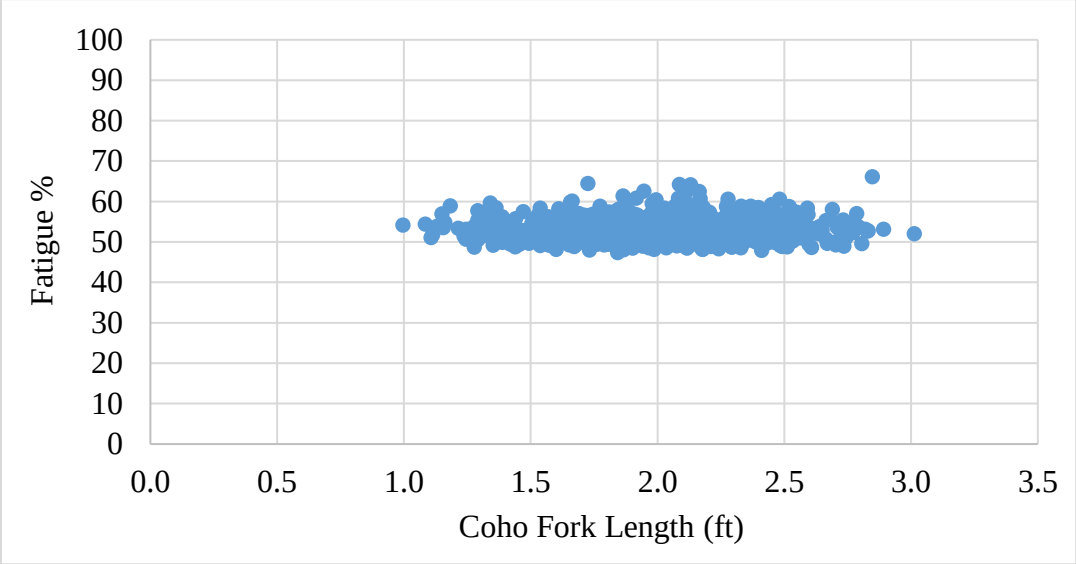

Figure 35. Plot of one thousand simulated Coho salmon and their percent fatigue from completing the ascension of the prototype fishway on the long pathway for the medium flow rate.

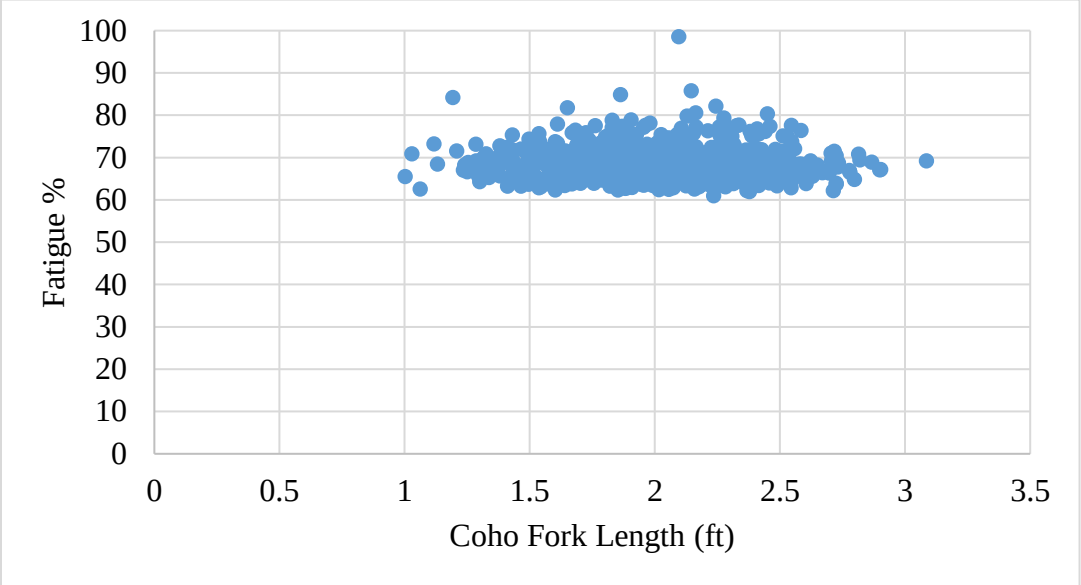

Figure 36. Plot of one thousand simulated Coho salmon and their percent fatigue from completing the ascension of an extended prototype fishway on the long pathway for the medium flow rate.

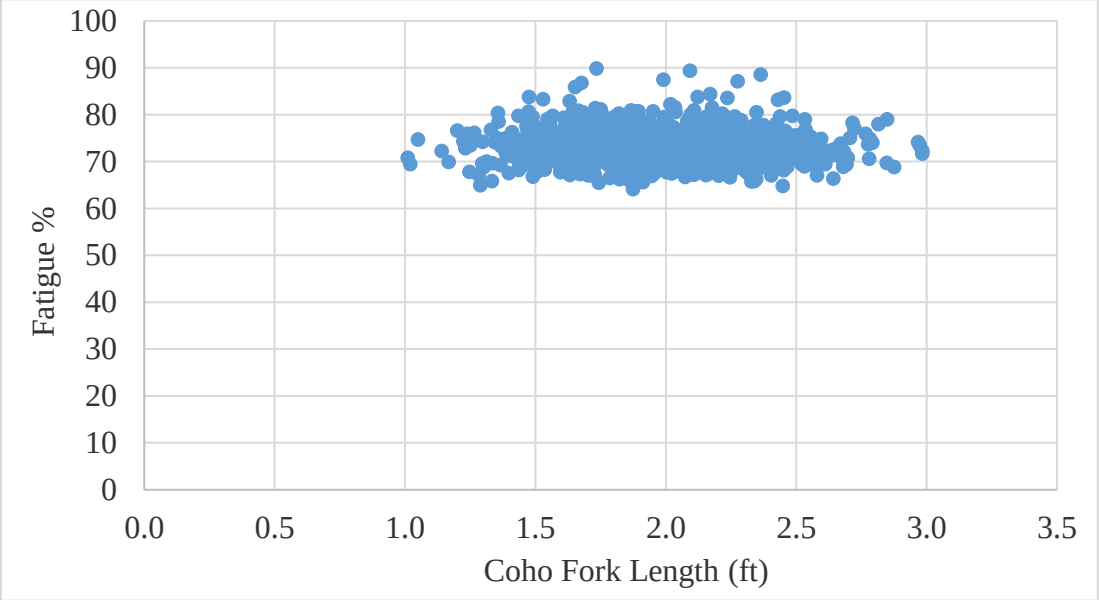

Figure 37. Plot of one thousand simulated Coho salmon and their percent fatigue from completing the ascension of an extended prototype fishway on the straight pathway for the high flow rate.

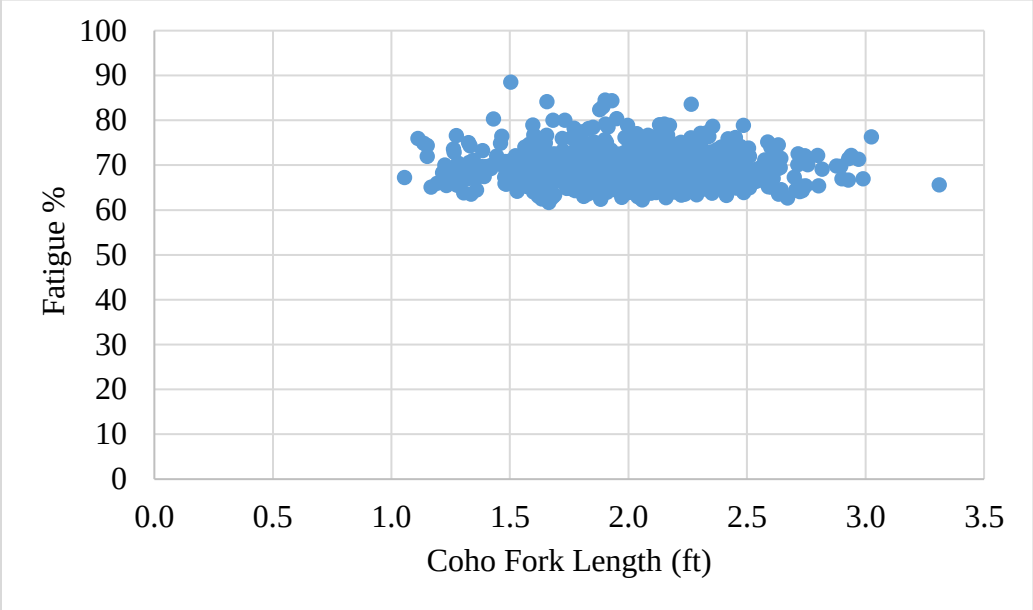

Figure 38. Plot of one thousand simulated Coho salmon and their percent fatigue from completing the ascension of an extended prototype fishway on the long pathway for the high flow rate.